Supporting Information

Implications of Indenyl Substitution for the Structural Chemistry of Rare-Earth-Metal (Half-) Sandwich Complexes and Performance in Living Isoprene Polymerization

Dominic Diether, Cäcilia Maichle-Mössmer, and Reiner Anwander*

Institut für Anorganische Chemie, Eberhard Karls Universität Tübingen, Auf der Morgenstelle 18, 72076 Tübingen, Germany.

Corresponding Author

* reiner.anwander@uni-tuebingen.de

Table of Contents

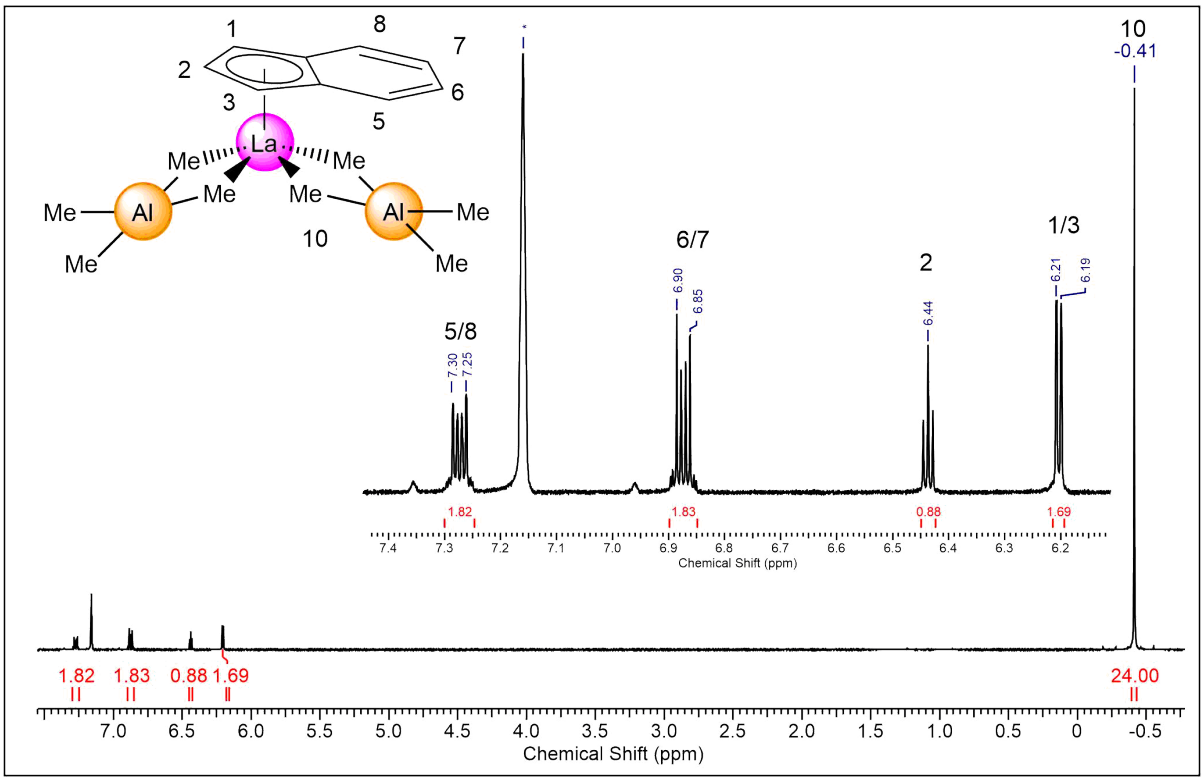

Figure S1. ^{1}H NMR spectrum (400 MHz) of (Ind)La(AlMe$_4$)$_2$ (**1a**) in C_6D_6 at 26 °C.

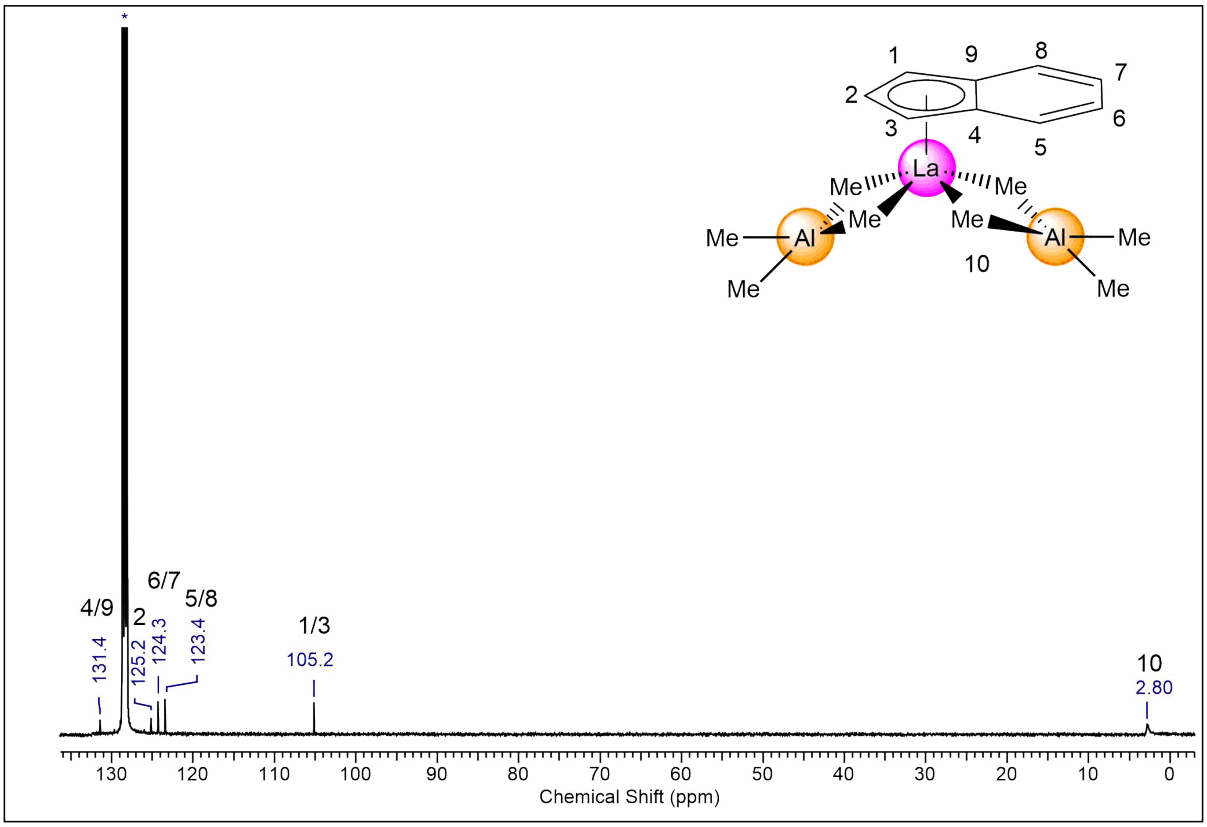

Figure S2. ^{13}C{^{1}H} NMR spectrum (101 MHz) of (Ind)La(AlMe$_4$)$_2$ (**1a**) in C_6D_6 at 26 °C.

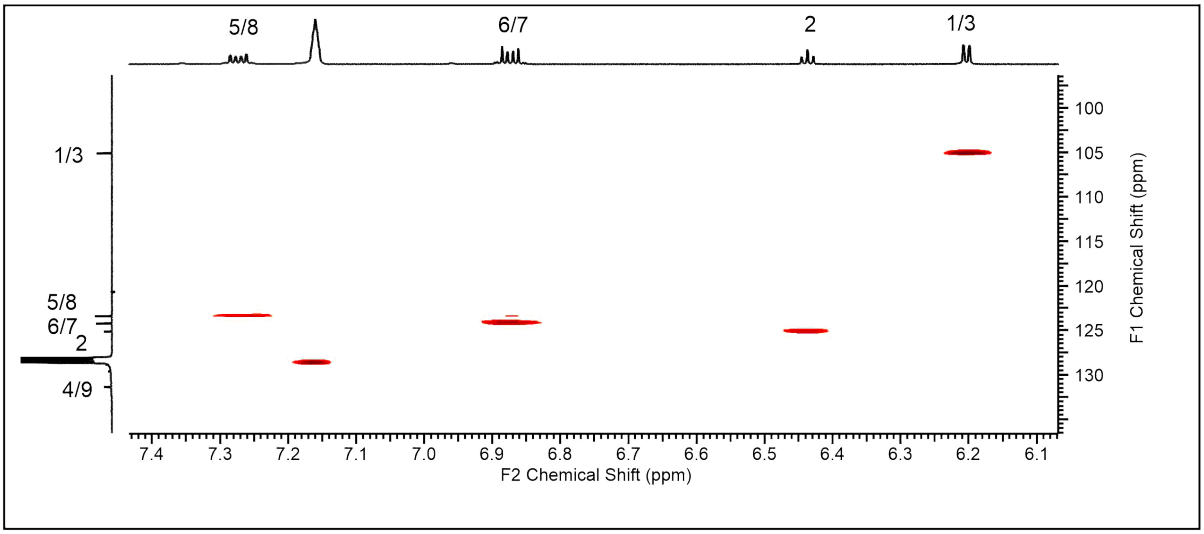

Figure S3. $^{1}H^{13}C$-HSQC NMR spectrum (400/101 MHz) of (Ind)La($AlMe_4$)$_2$ (**1a**) in C_6D_6 at 26 °C.

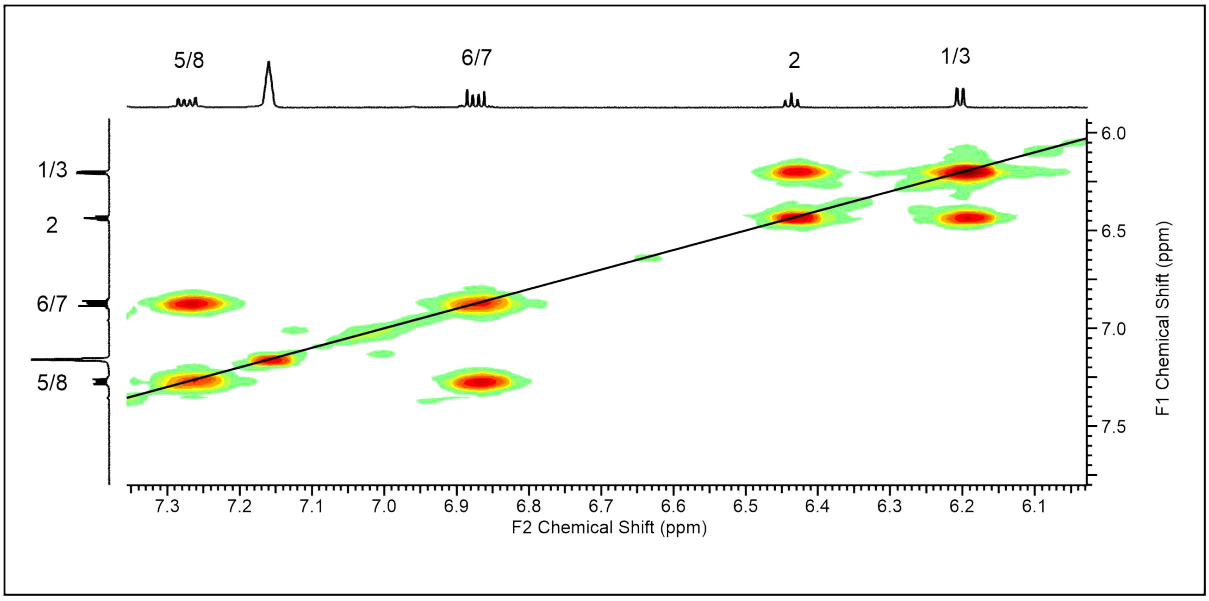

Figure S4. Section of the $^{1}H^{1}H$-COSY NMR spectrum (400/400 MHz) of (Ind)La($AlMe_4$)$_2$ (**1a**) in C_6D_6 at 26 °C.

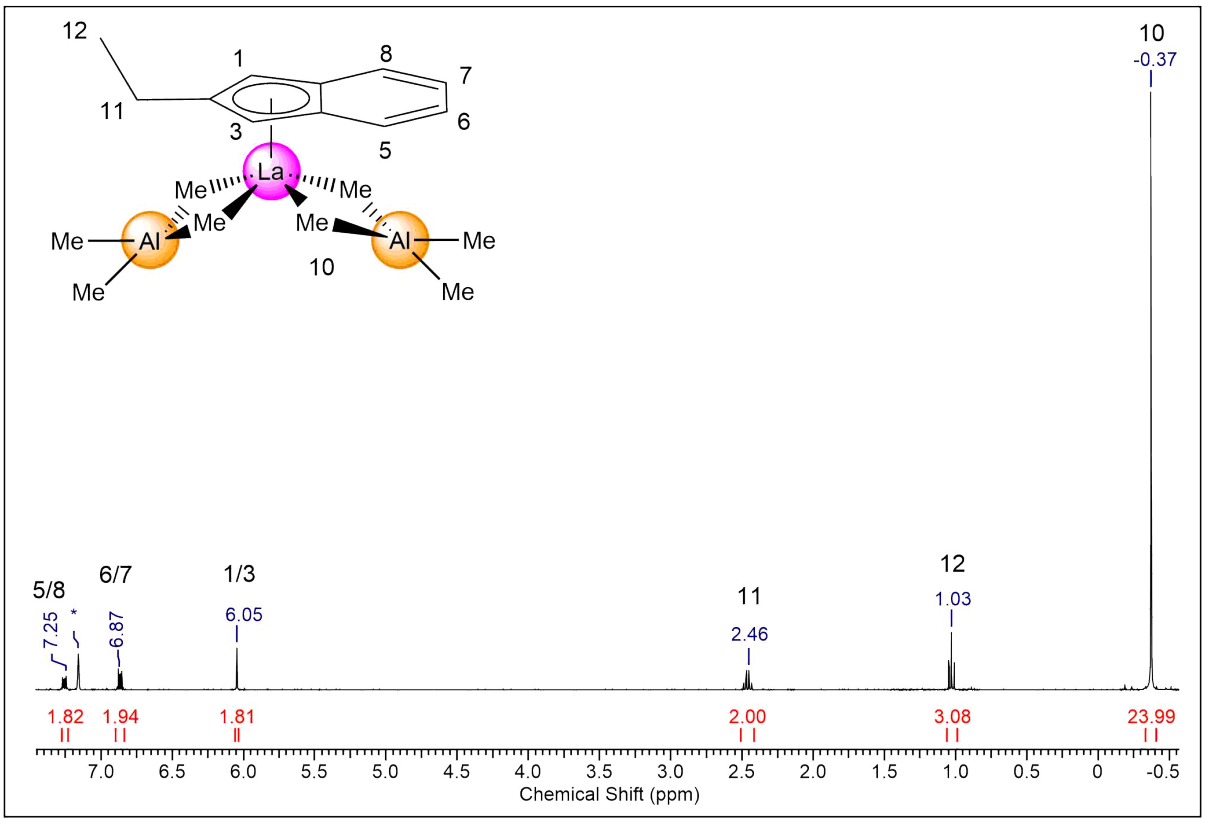

Figure S5. ^{1}H NMR spectrum (400 MHz) of (Ind^{Et})La(AlMe$_4$)$_2$ (**1b**) in C_6D_6 at 26 °C.

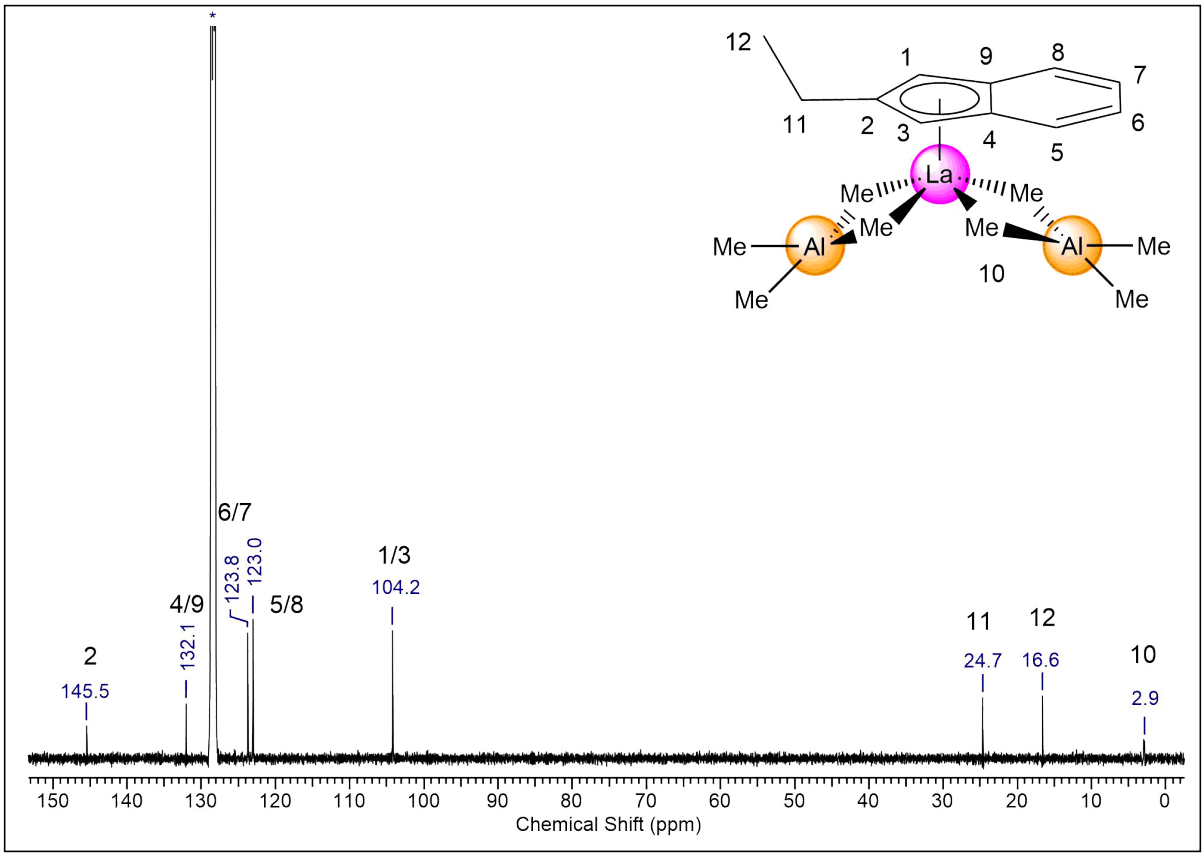

Figure S6. ^{13}C{^{1}H} NMR spectrum (101 MHz) of (Ind^{Et})La(AlMe$_4$)$_2$ (**1b**) in C_6D_6 at 26 °C.

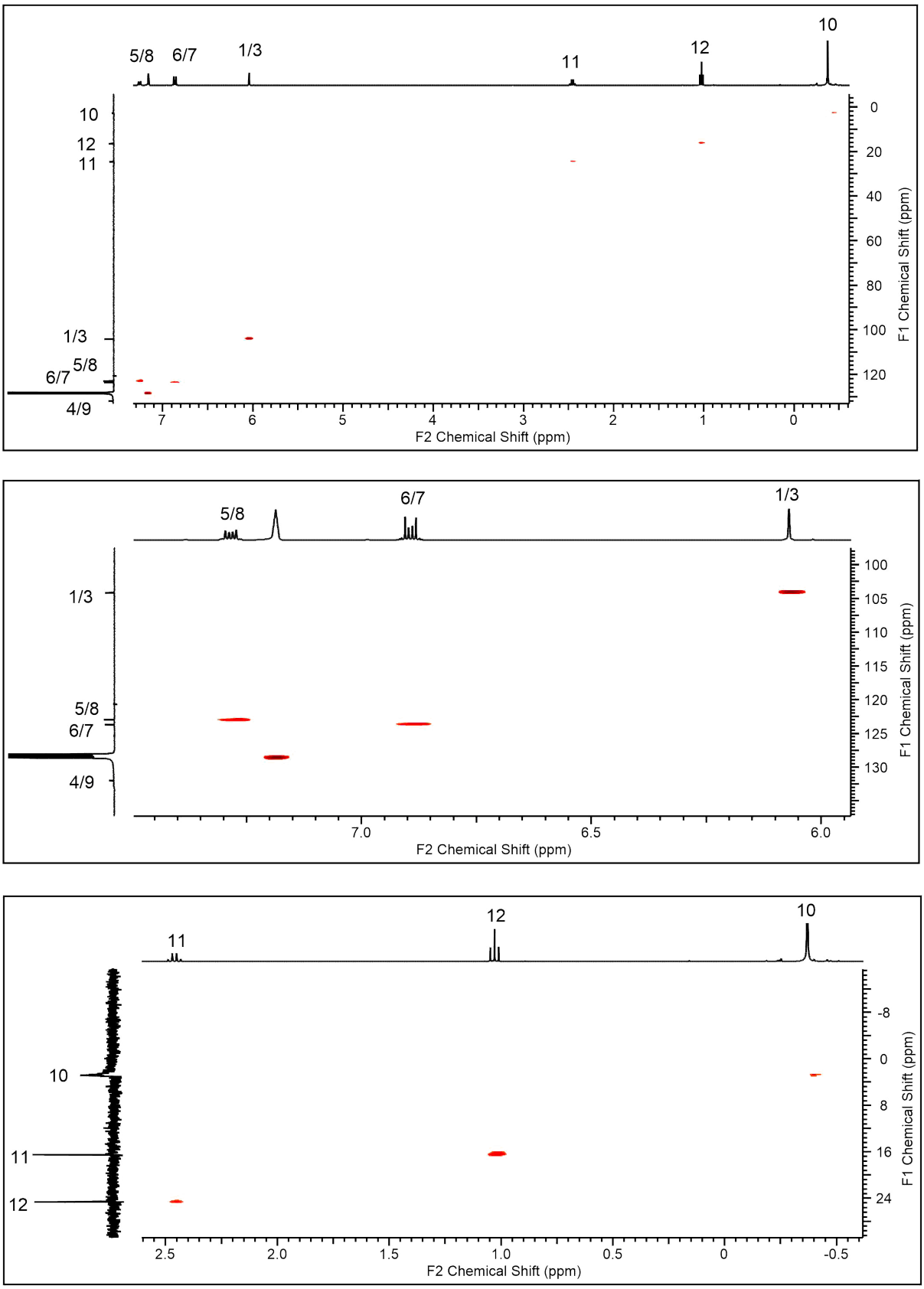

Figure S7. $^{1}H^{13}C$-HSQC NMR spectrum (400/101 MHz) of $(Ind^{Et})La(AlMe_4)_2$ (**1b**) in C_6D_6 at 26 °C, including enlarged sections.

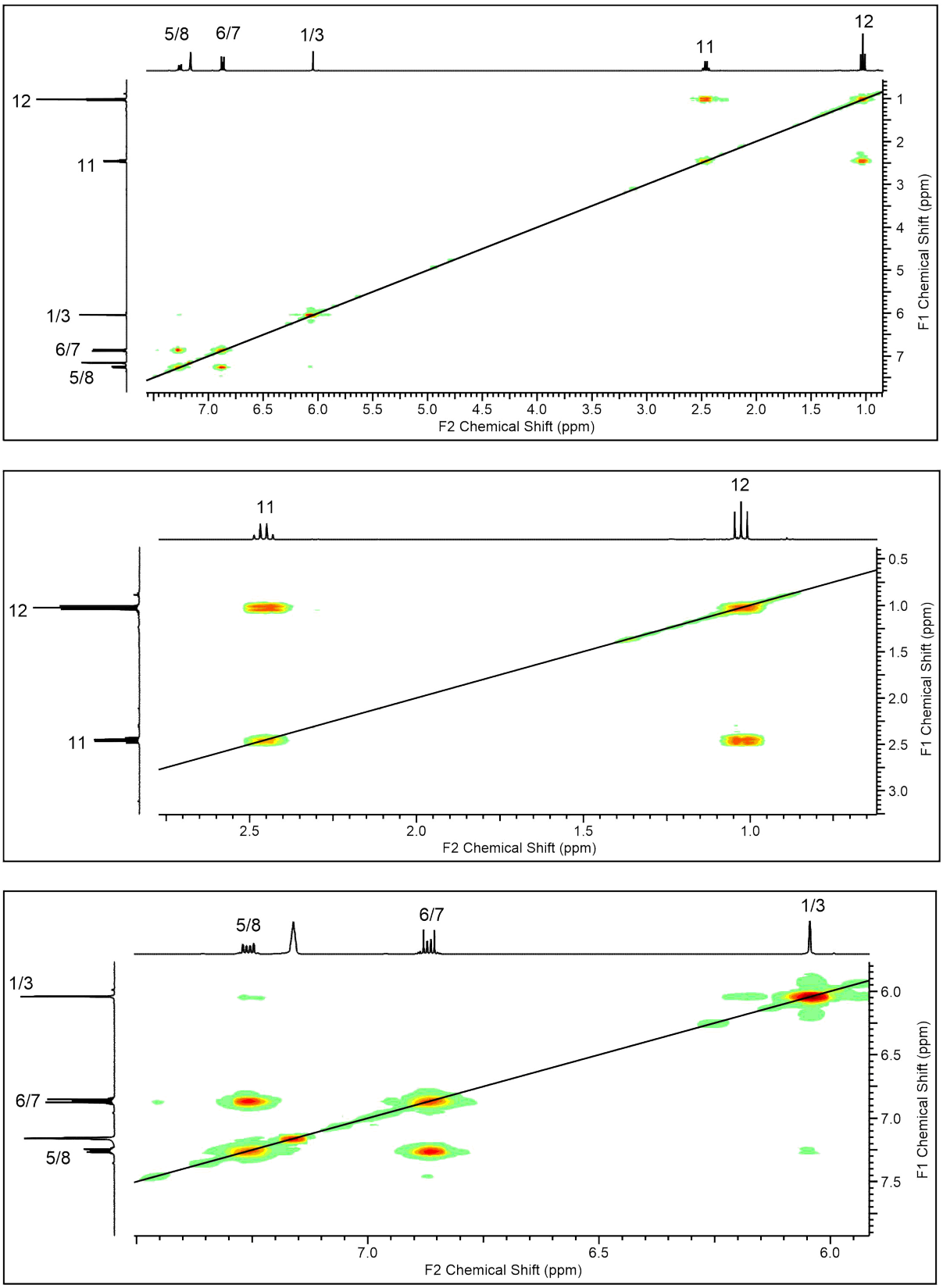

Figure S8. $^{1}H^{1}H$-COSY NMR spectrum (400/400 MHz) of (Ind^{Et})La($AlMe_4$)$_2$ (**1b**) in C_6D_6 at 26 °C, including enlarged sections.

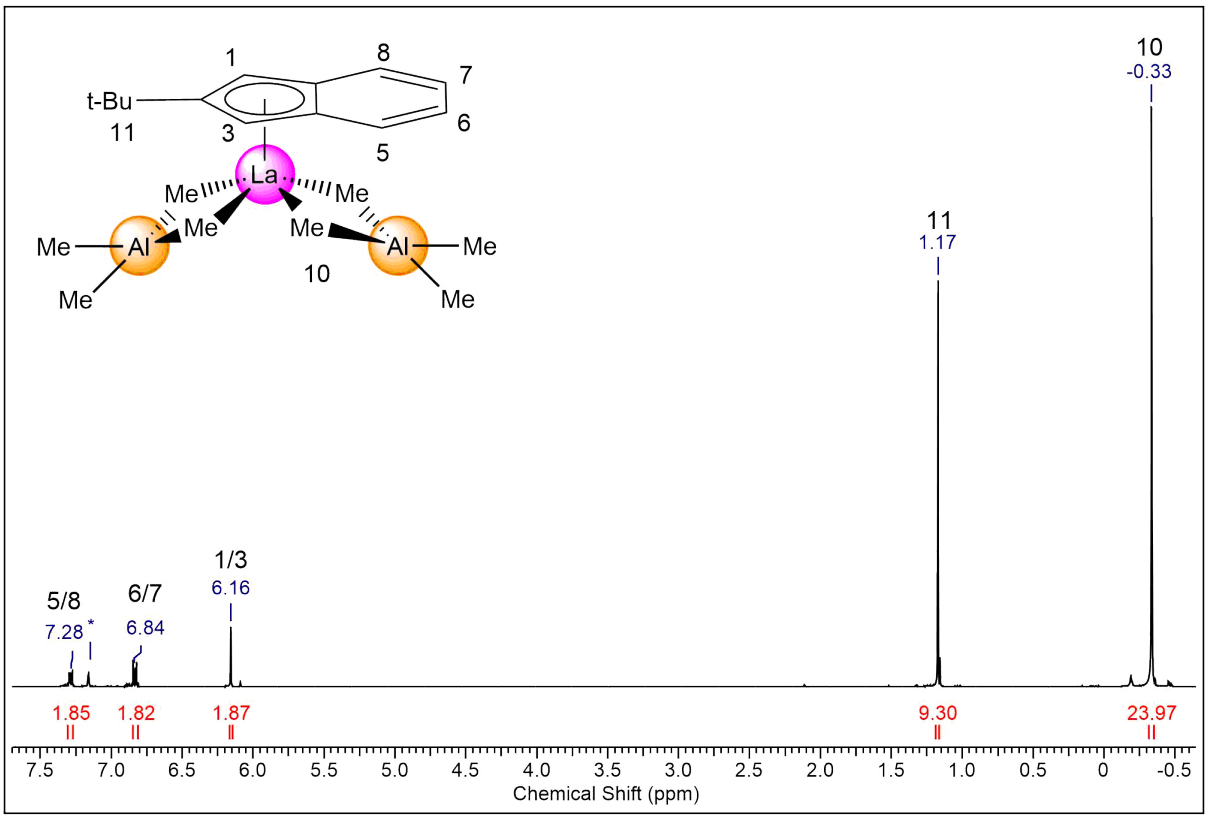

Figure S9. ^{1}H NMR spectrum (400 MHz) of (Ind$^{t\mathrm{Bu}}$)La(AlMe$_4$)$_2$ (**1c**) in C_6D_6 at 26 °C.

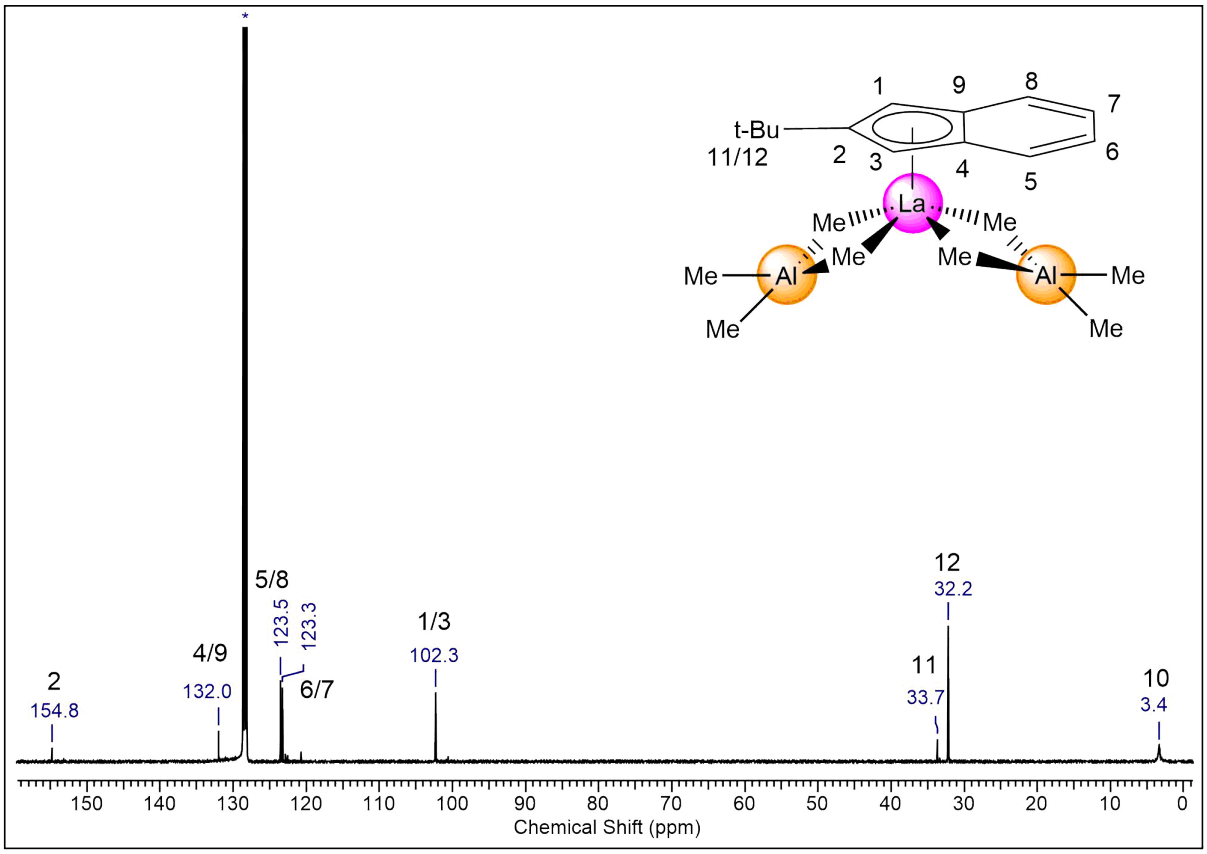

Figure S10. ^{13}C{^{1}H} NMR spectrum (101 MHz) of (Ind$^{t\mathrm{Bu}}$)La(AlMe$_4$)$_2$ (**1c**) in C_6D_6 at 26 °C.

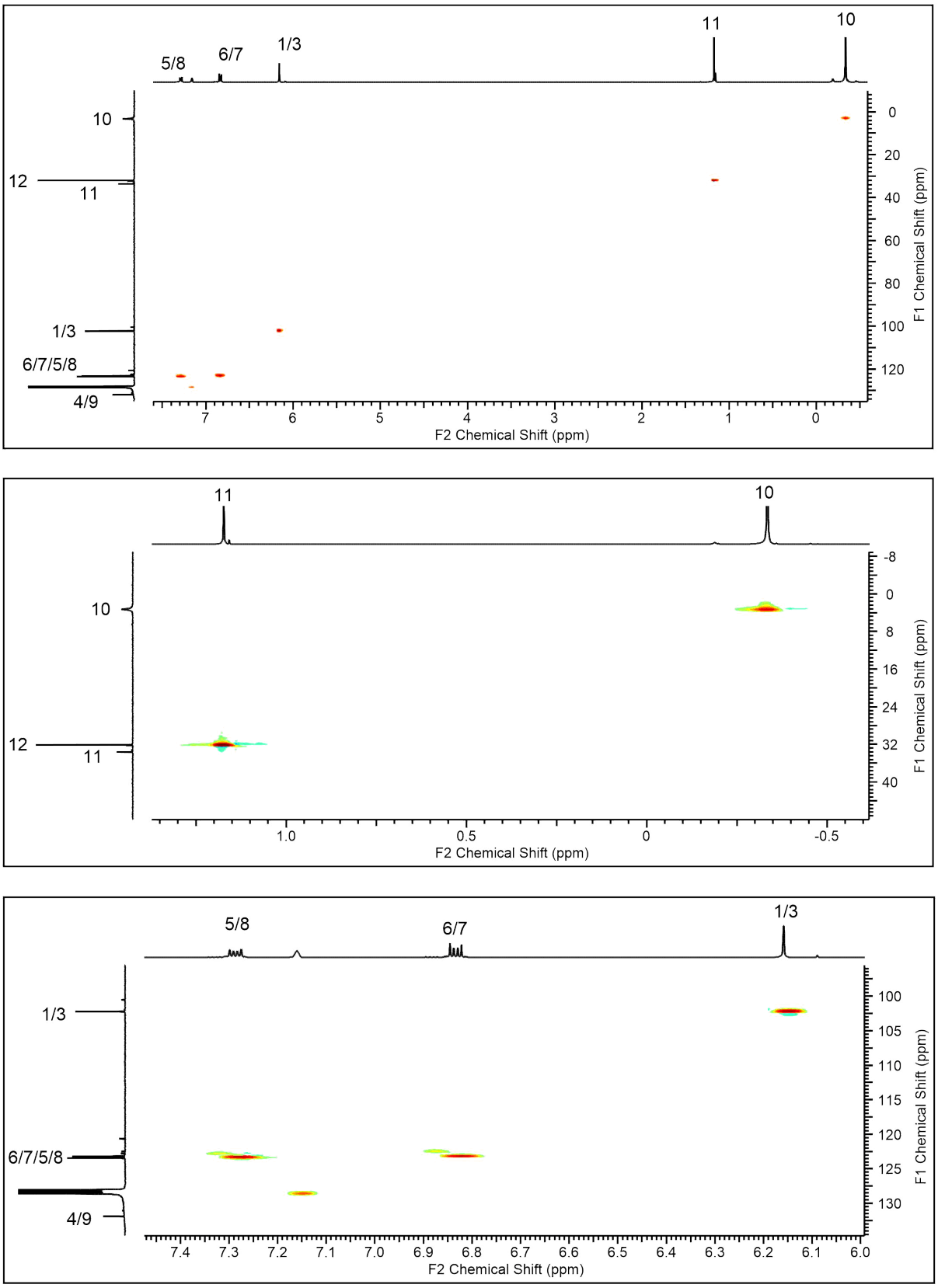

Figure S11. $^{1}H^{13}C$-HSQC NMR spectrum (400/101 MHz) of (Ind^{tBu})La(AlMe$_4$)$_2$ (**1c**) in C_6D_6 at 26 °C, including enlarged sections.

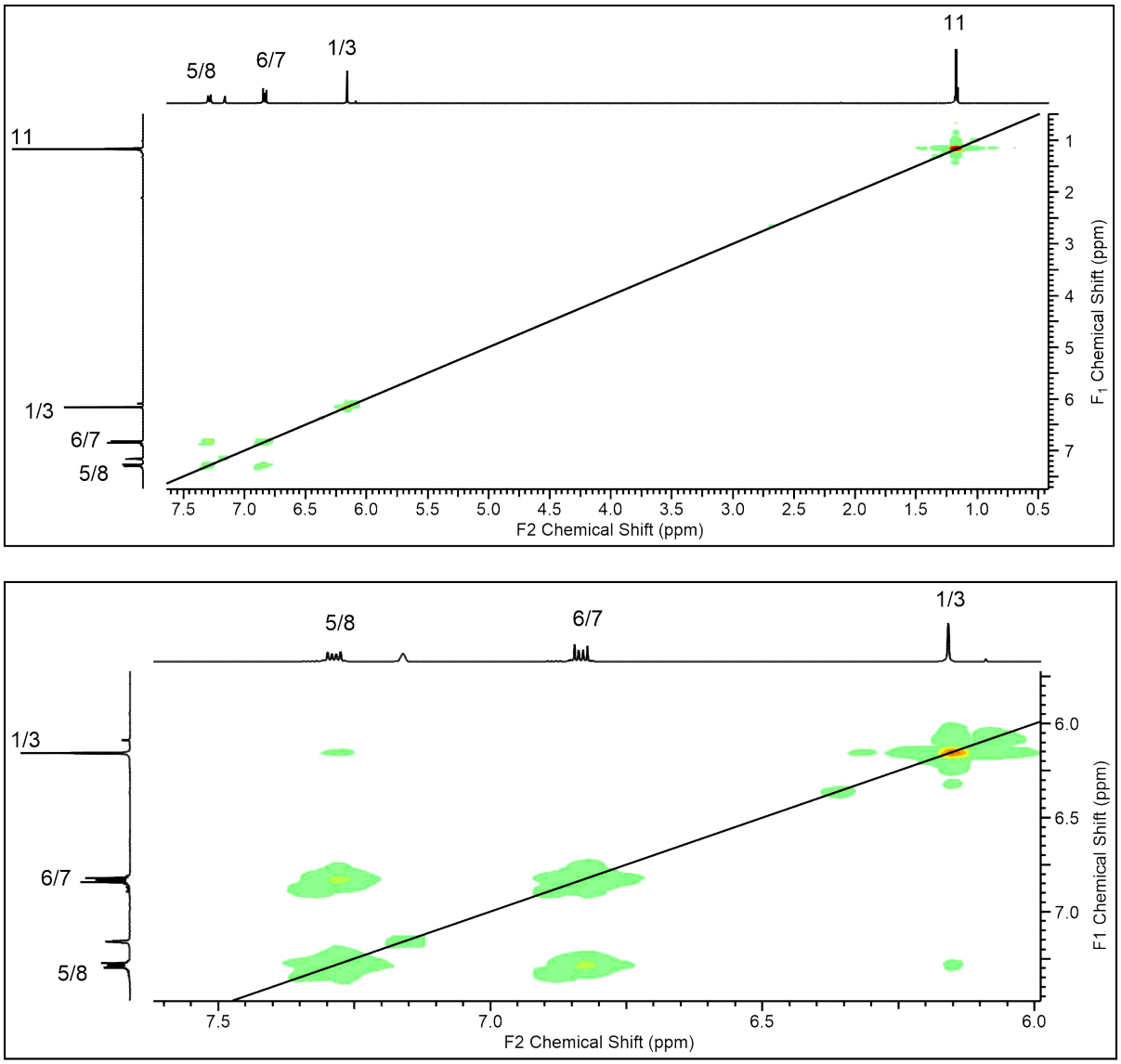

Figure S12. $^{1}H^{1}H$-COSY NMR spectrum (400/400 MHz) of (Ind^{tBu})La(AlMe$_4$)$_2$ (**1c**) in C_6D_6 at 26 °C, including an enlarged section.

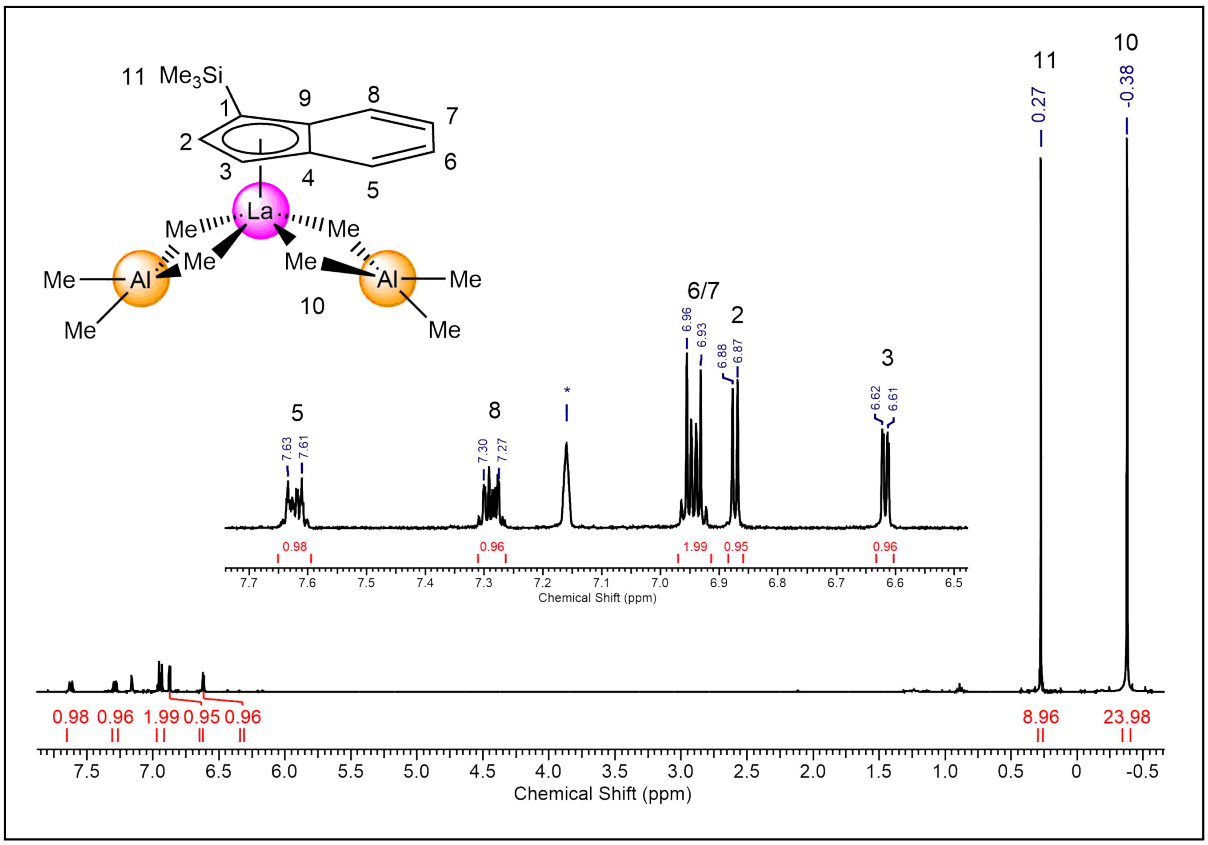

Figure S13. ^{1}H NMR spectrum (400 MHz) of (Ind^{Si})La(AlMe$_4$)$_2$ (**1d**) in C_6D_6 at 26 °C.

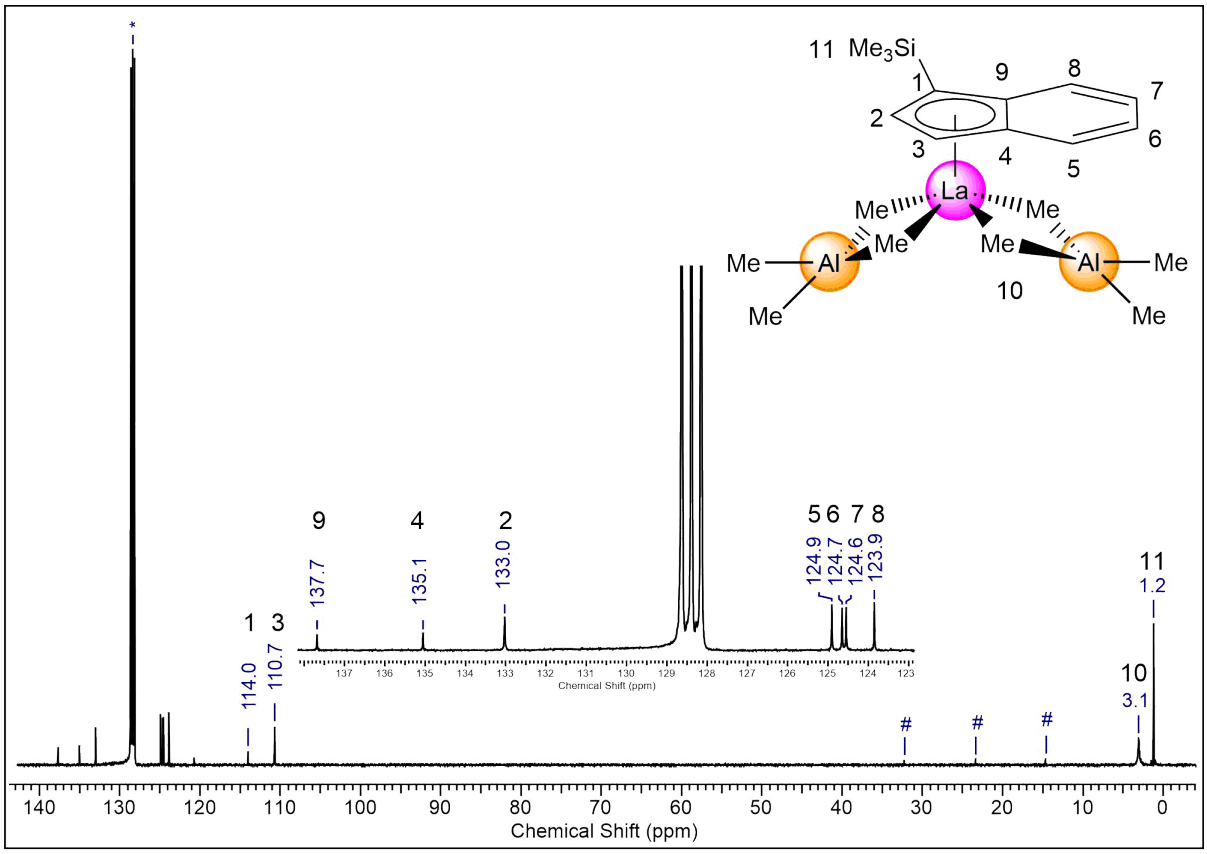

Figure S14. ^{13}C{^{1}H} NMR spectrum (101 MHz) of (Ind^{Si})La(AlMe$_4$)$_2$ (**1d**) in C_6D_6 at 26 °C. Residual *n*-hexane marked with #.

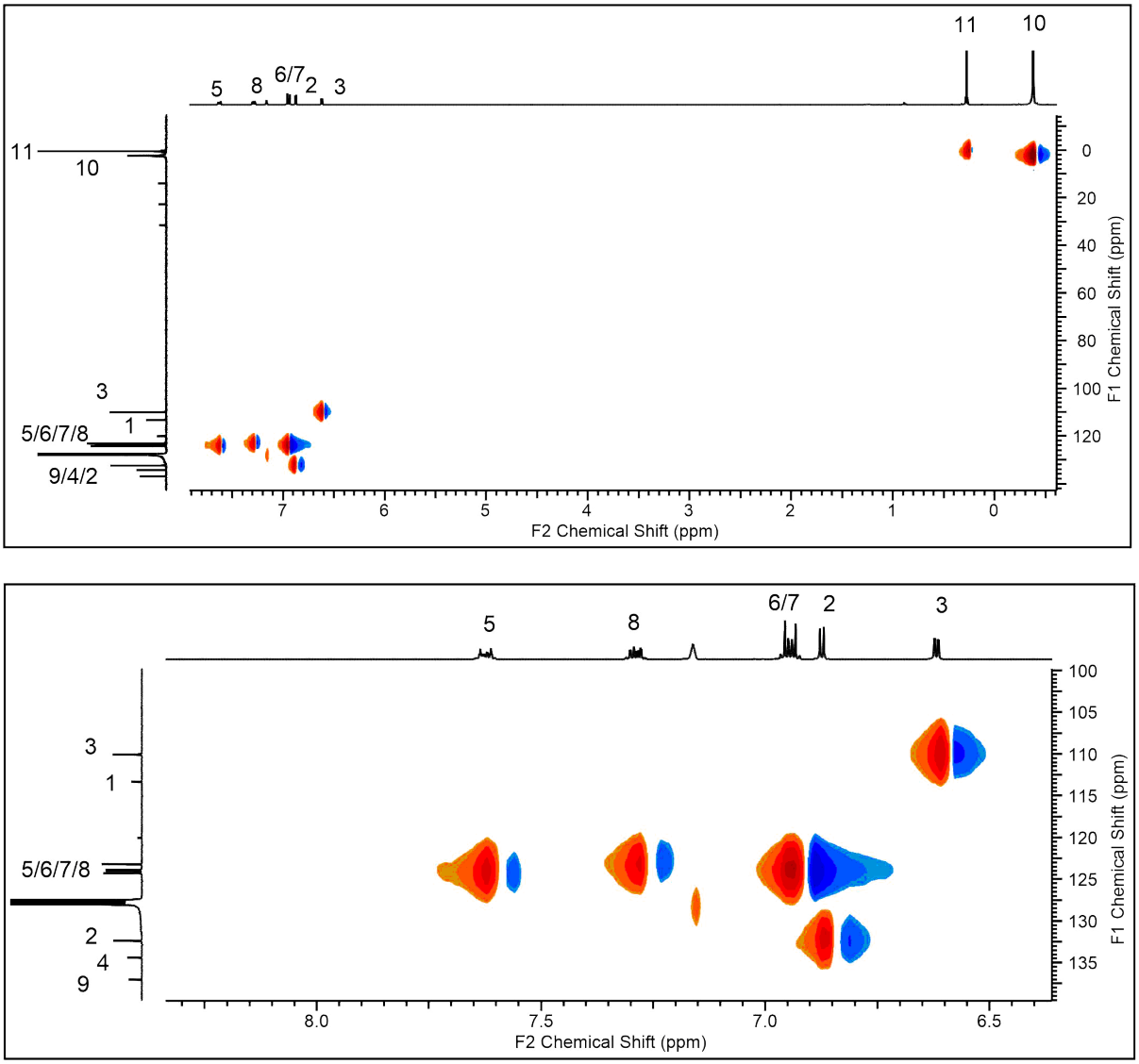

Figure S15. $^{1}H^{13}C$-HSQC NMR spectrum (400/101 MHz) of $(Ind^{Si})La(AlMe_4)_2$ (**1d**) in C_6D_6 at 26 °C, including an enlarged section.

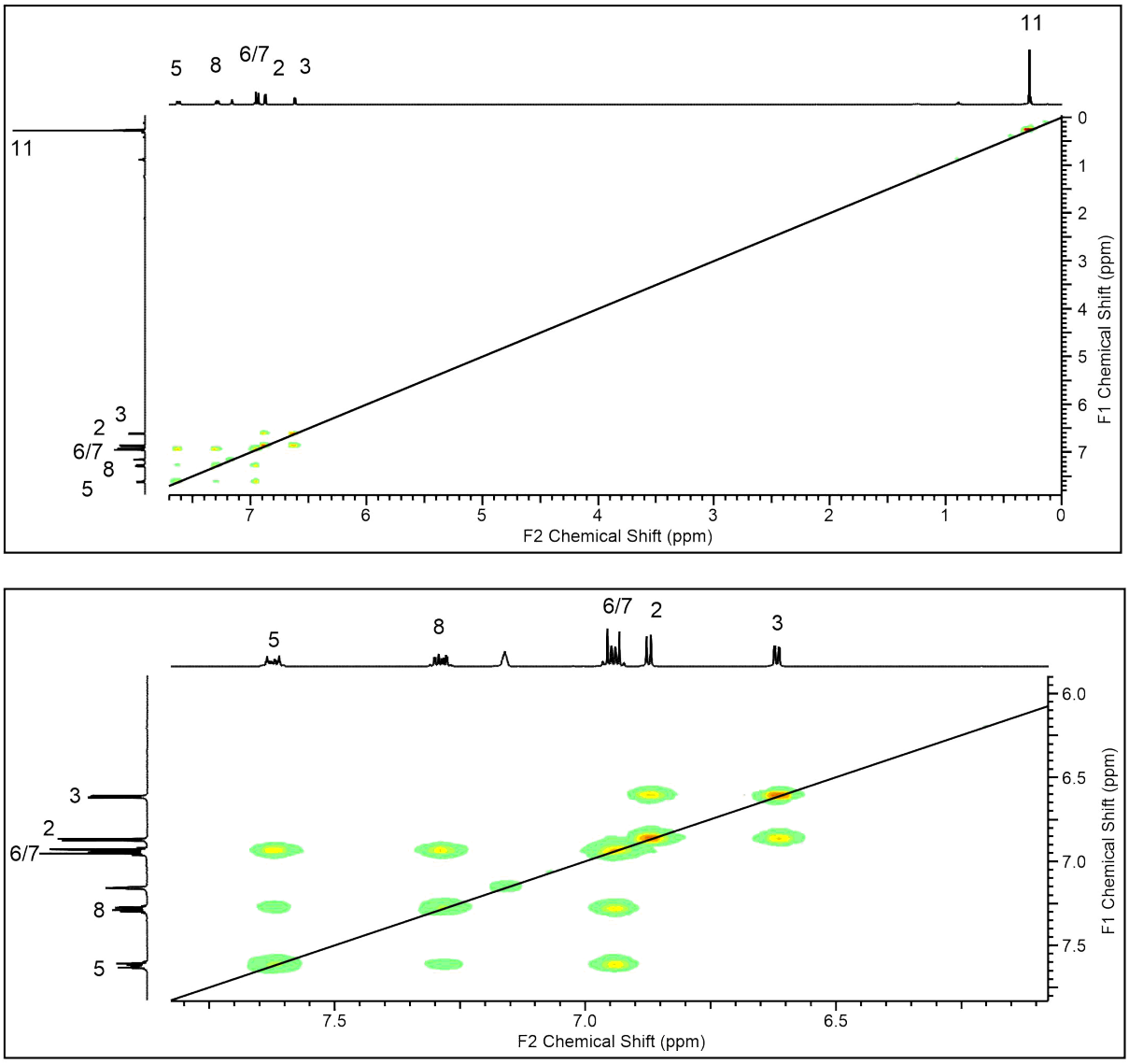

Figure S16. $^{1}H^{1}H$-COSY NMR spectrum (400/400 MHz) of $(Ind^{Si})La(AlMe_4)_2$ (**1d**) in C_6D_6 at 26 °C, including an enlarged section.

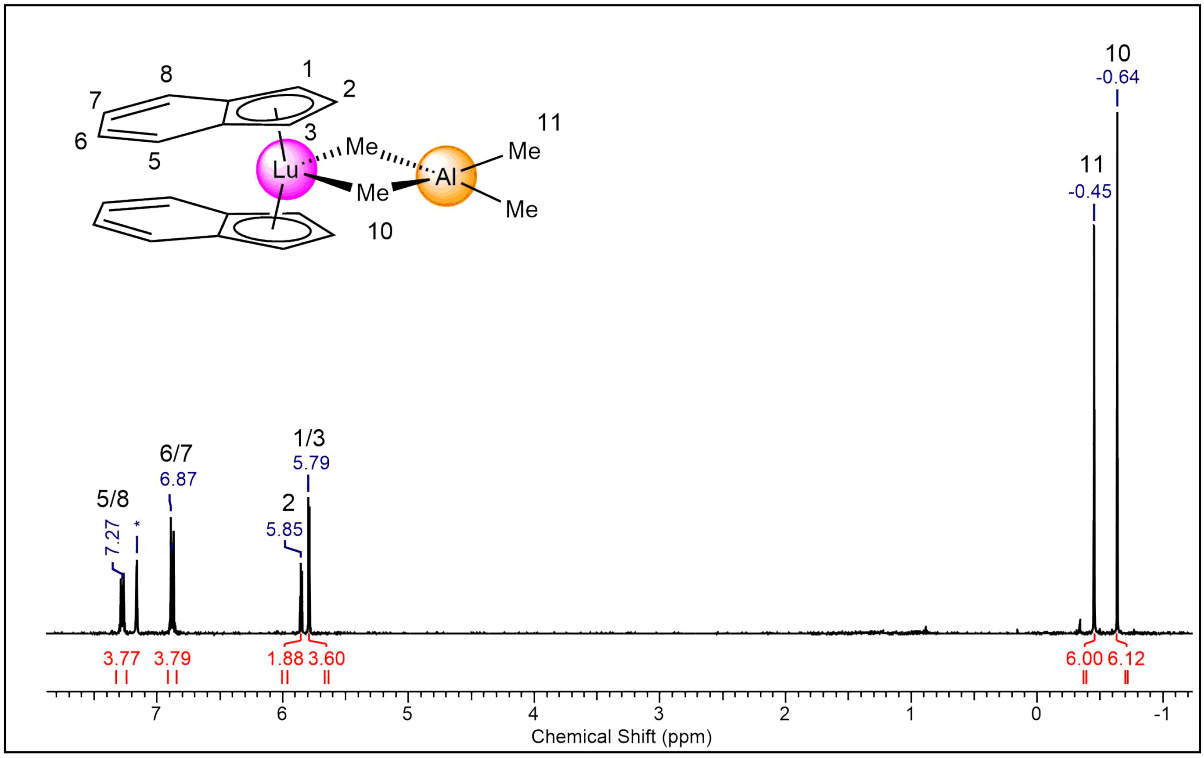

Figure S17. ^{1}H NMR spectrum (400 MHz) of $(Ind)_2Lu(AlMe_4)$ (**2a**) in C_6D_6 at 26 °C.

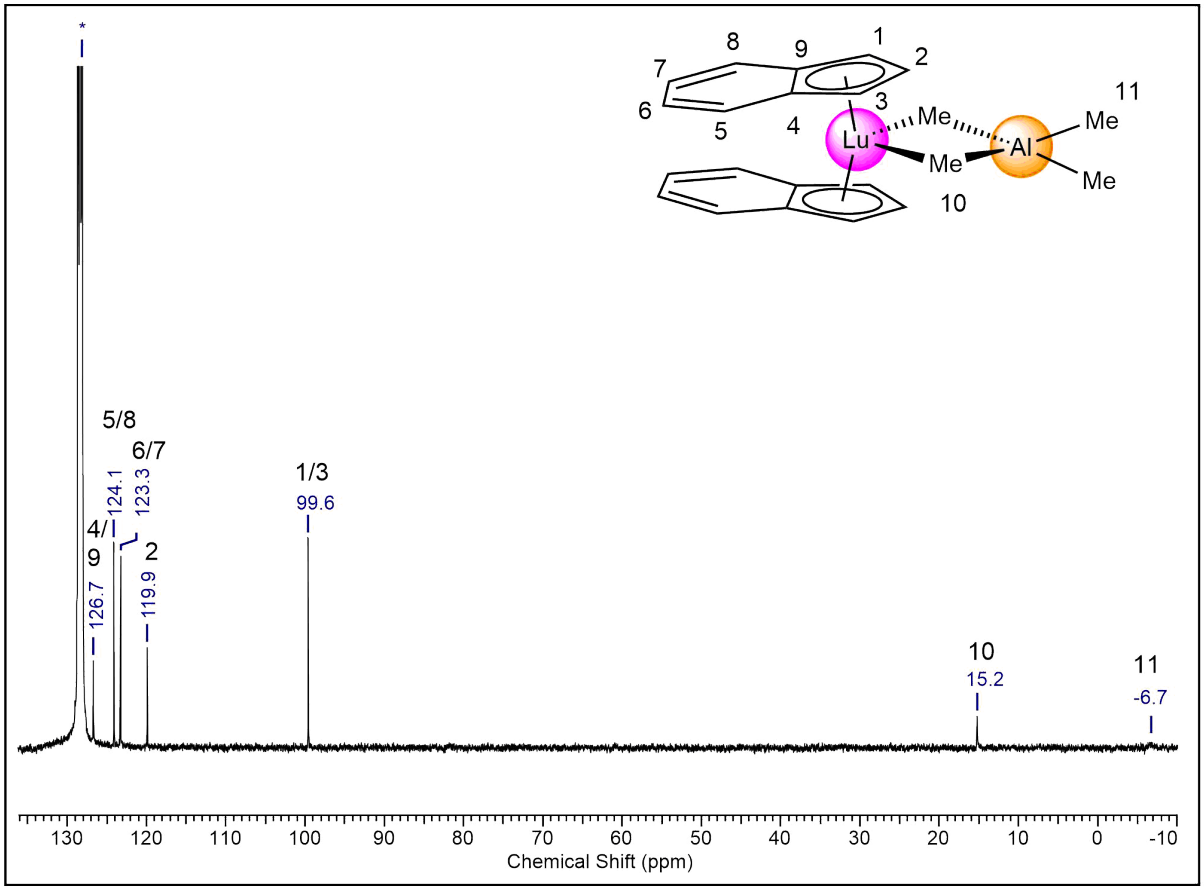

Figure S18. ^{13}C{^{1}H} NMR spectrum (101 MHz) of $(Ind)_2Lu(AlMe_4)$ (**2a**) in C_6D_6 at 26 °C.

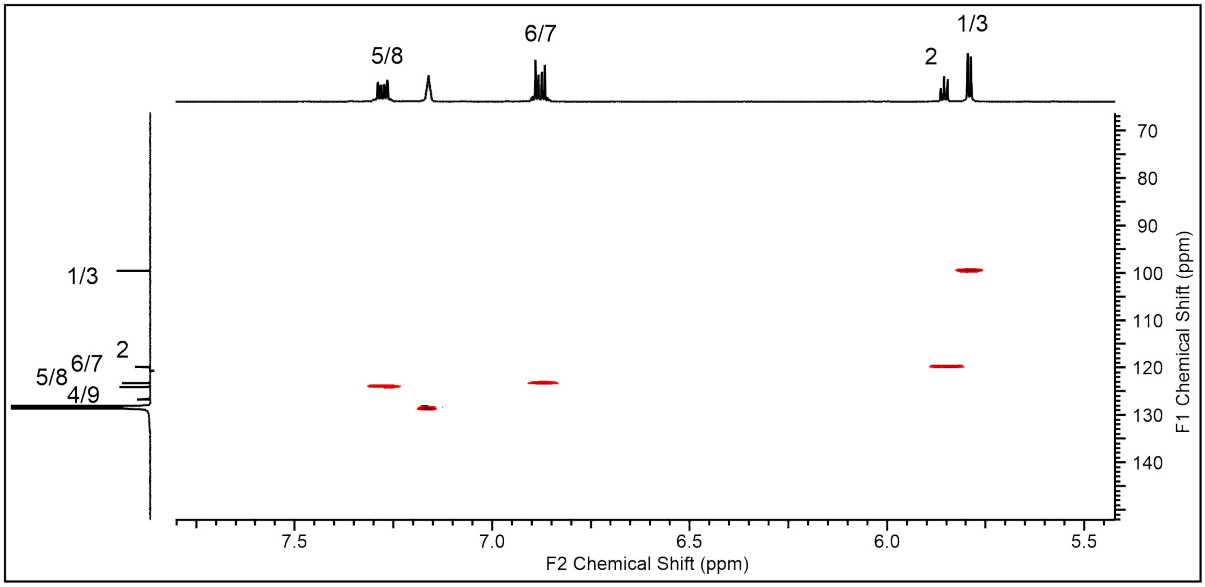

Figure S19. Section of the $^{1}H^{13}C$-HSQC NMR spectrum (400/101 MHz) of $(Ind)_2Lu(AlMe_4)$ (**2a**) in C_6D_6 at 26 °C.

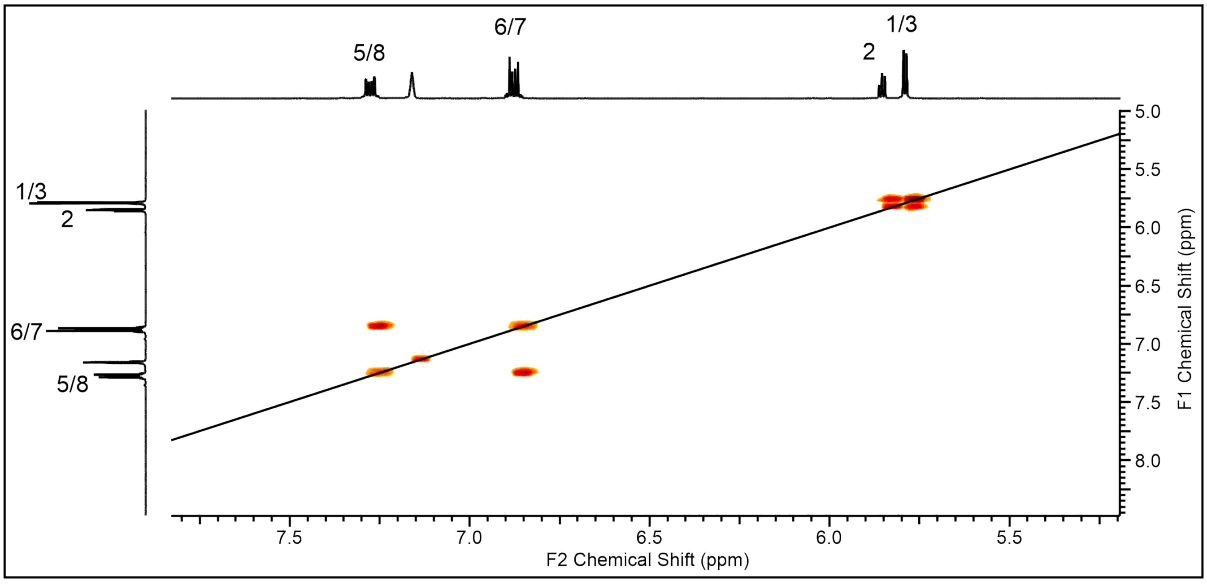

Figure S20. Section of the $^{1}H^{1}H$-COSY NMR spectrum (400/400 MHz) of $(Ind)_2Lu(AlMe_4)$ (**2a**) in C_6D_6 at 26 °C.

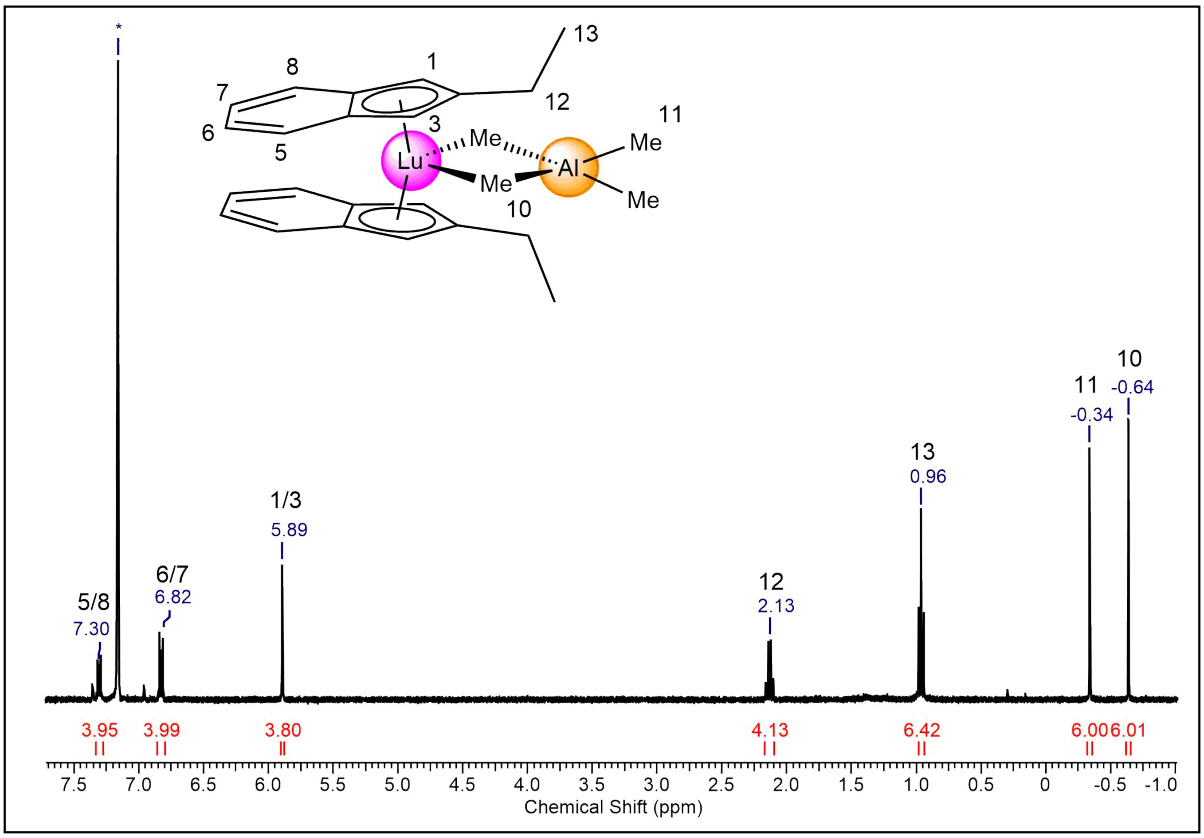

Figure S21. ^{1}H NMR spectrum (400 MHz) of $(Ind^{Et})_2Lu(AlMe_4)$ (**2b**) in C_6D_6 at 26 °C.

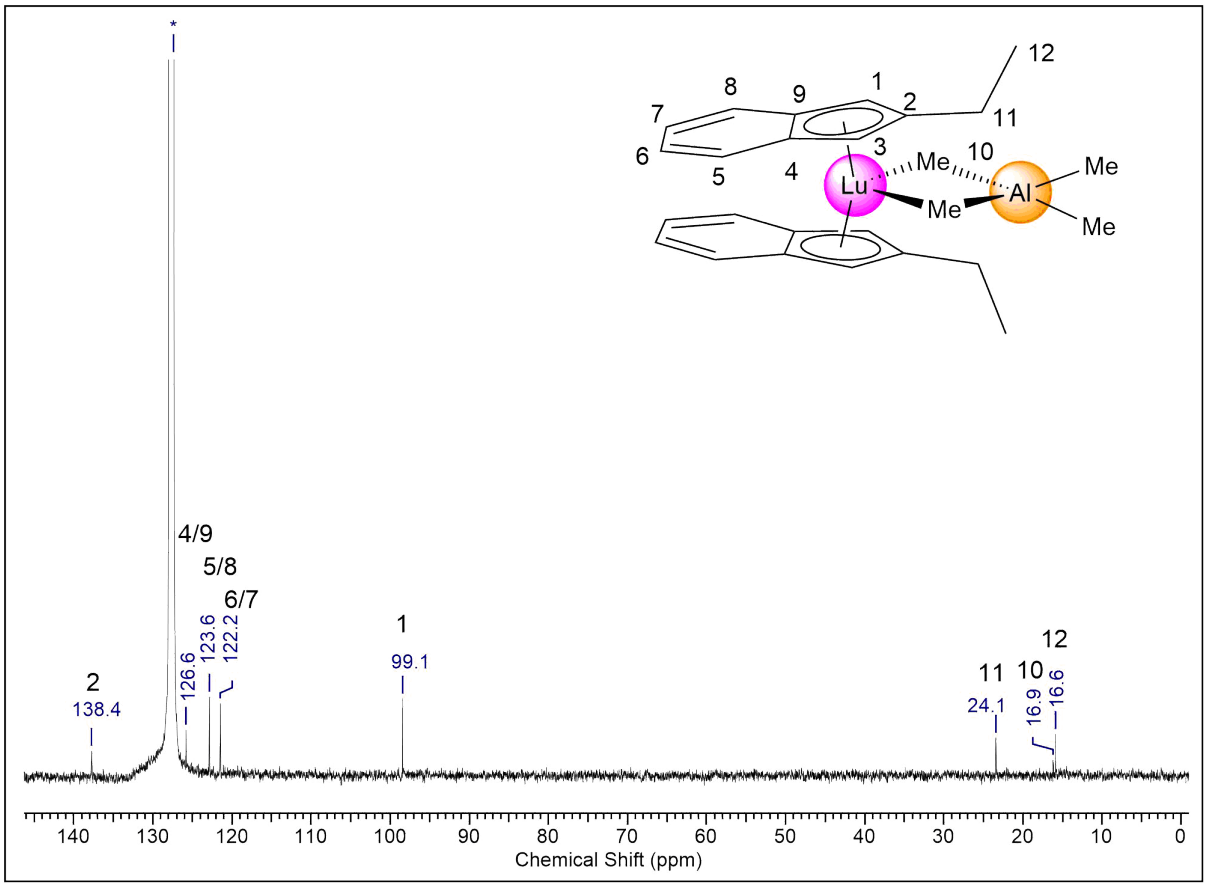

Figure S22. $^{13}C\{^{1}H\}$ NMR spectrum (101 MHz) of $(Ind^{Et})_2Lu(AlMe_4)$ (**2b**) in C_6D_6 at 26 °C.

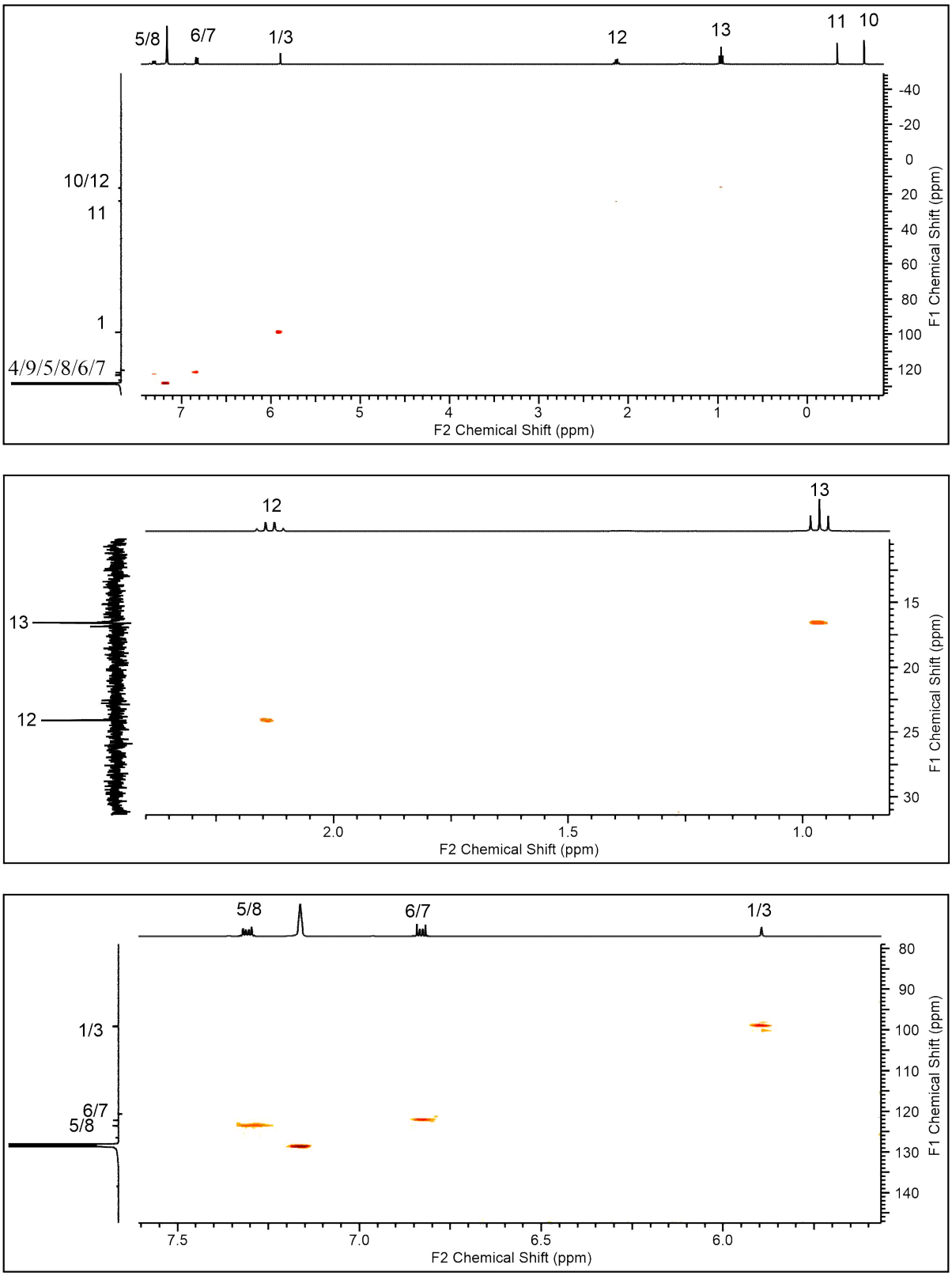

Figure S23. $^{1}H^{13}C$-HSQC NMR spectrum (400/101 MHz) of $(Ind^{Et})_2La(AlMe_4)$ (**2b**) in C_6D_6 at 26 °C, including enlarged sections.

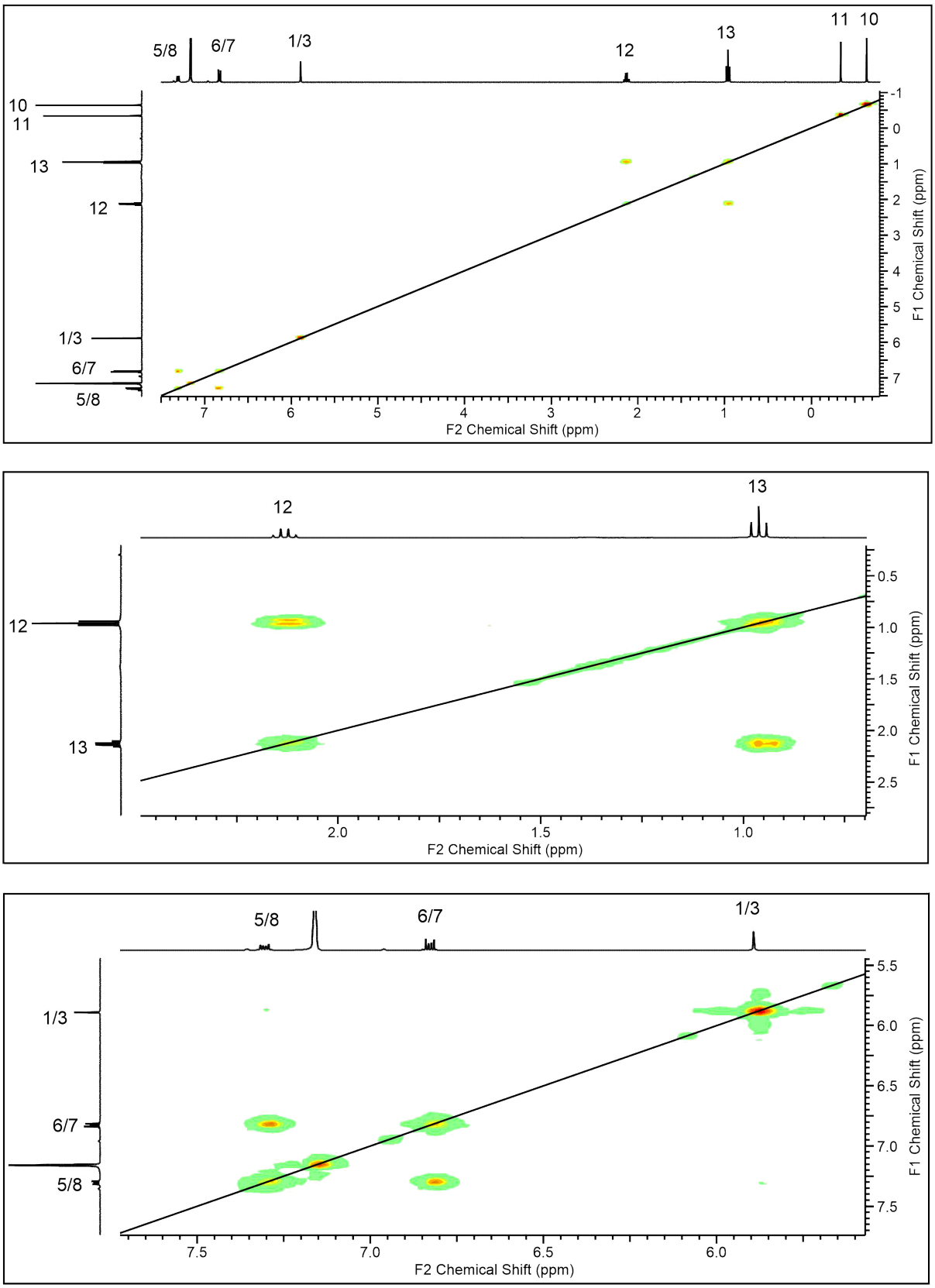

Figure S24. $^{1}H^{1}H$-COSY NMR spectrum (400/400 MHz) of $(Ind^{Et})_2Lu(AlMe_4)$ (**2b**) in C_6D_6 at 26 °C, including enlarged sections.

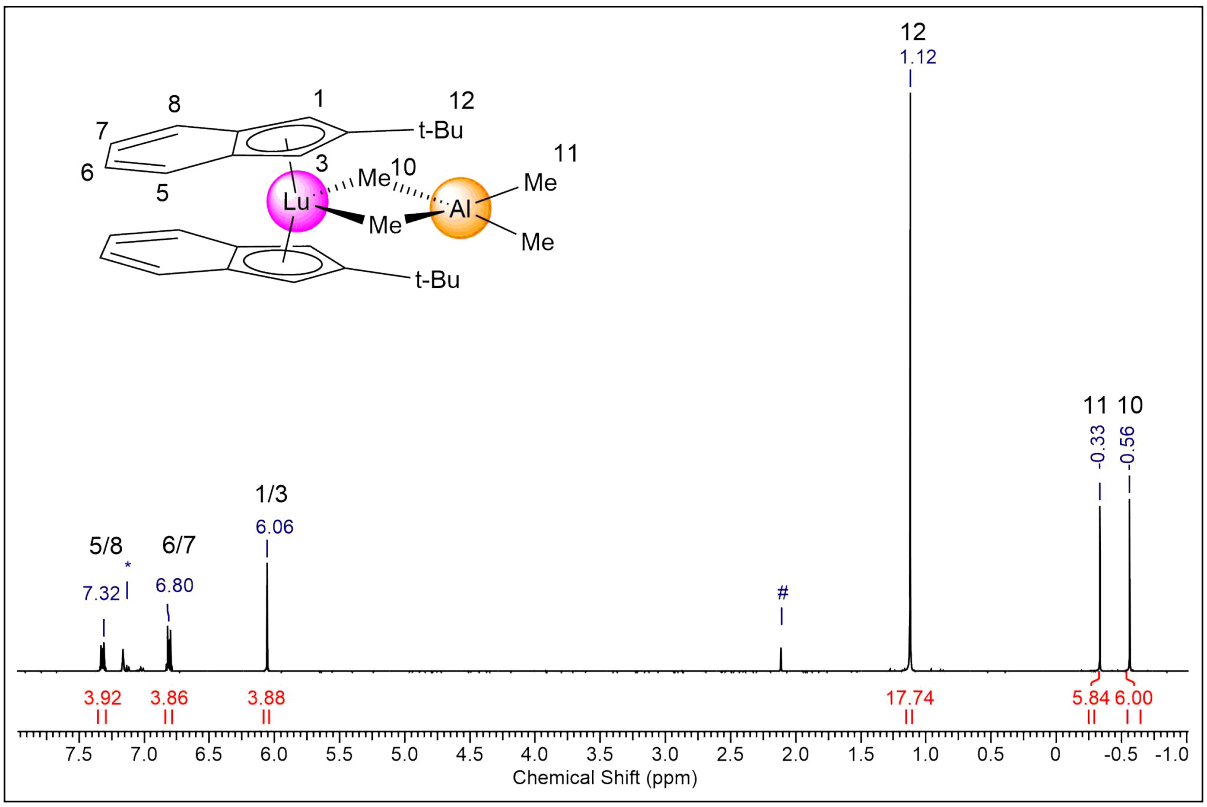

Figure S25. ^{1}H NMR spectrum (400 MHz) of $(Ind^{tBu})_2Lu(AlMe_4)$ (**2c**) in C_6D_6 at 26 °C. Residual toluene marked with #.

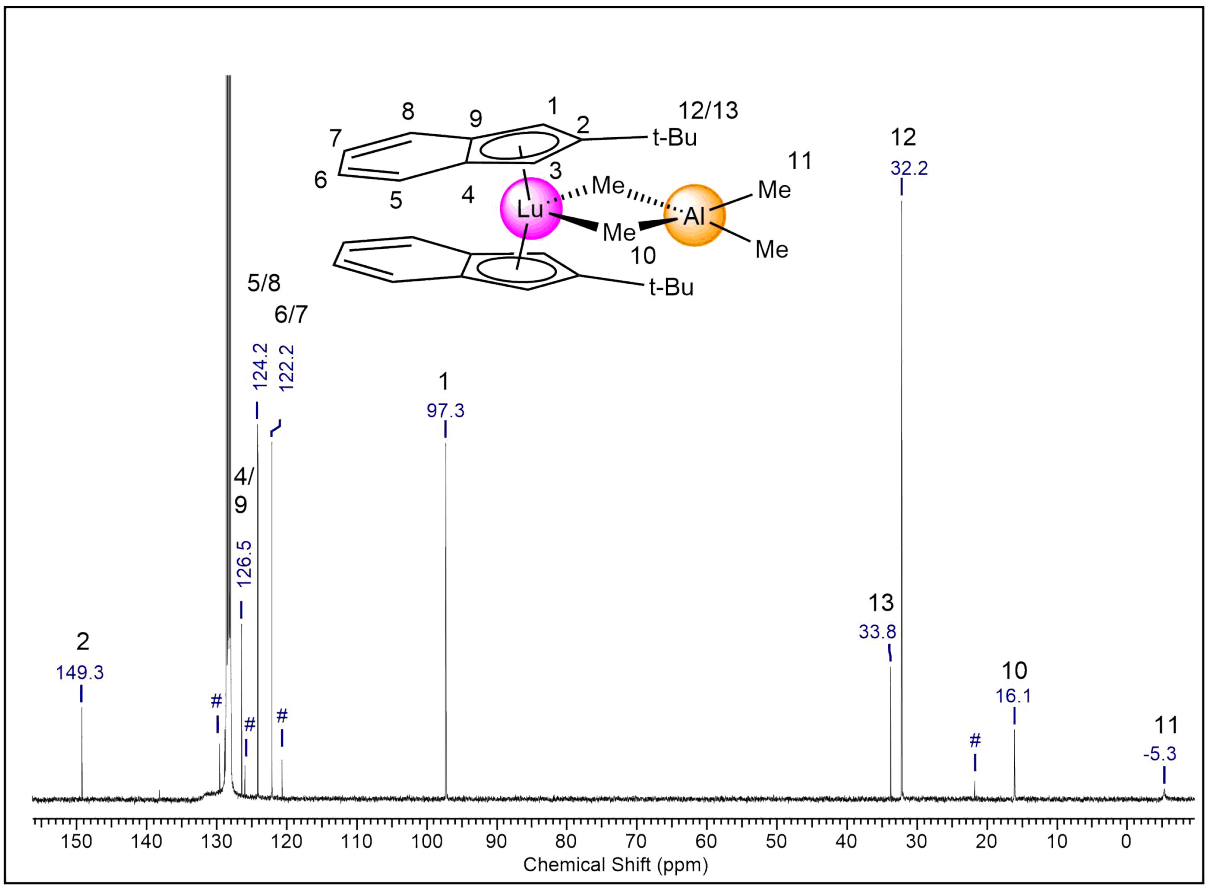

Figure S26. $^{13}C\{^{1}H\}$ NMR spectrum (101 MHz) of $(Ind^{tBu})_2Lu(AlMe_4)$ (**2c**) in C_6D_6 at 26 °C. Residual toluene marked with #.

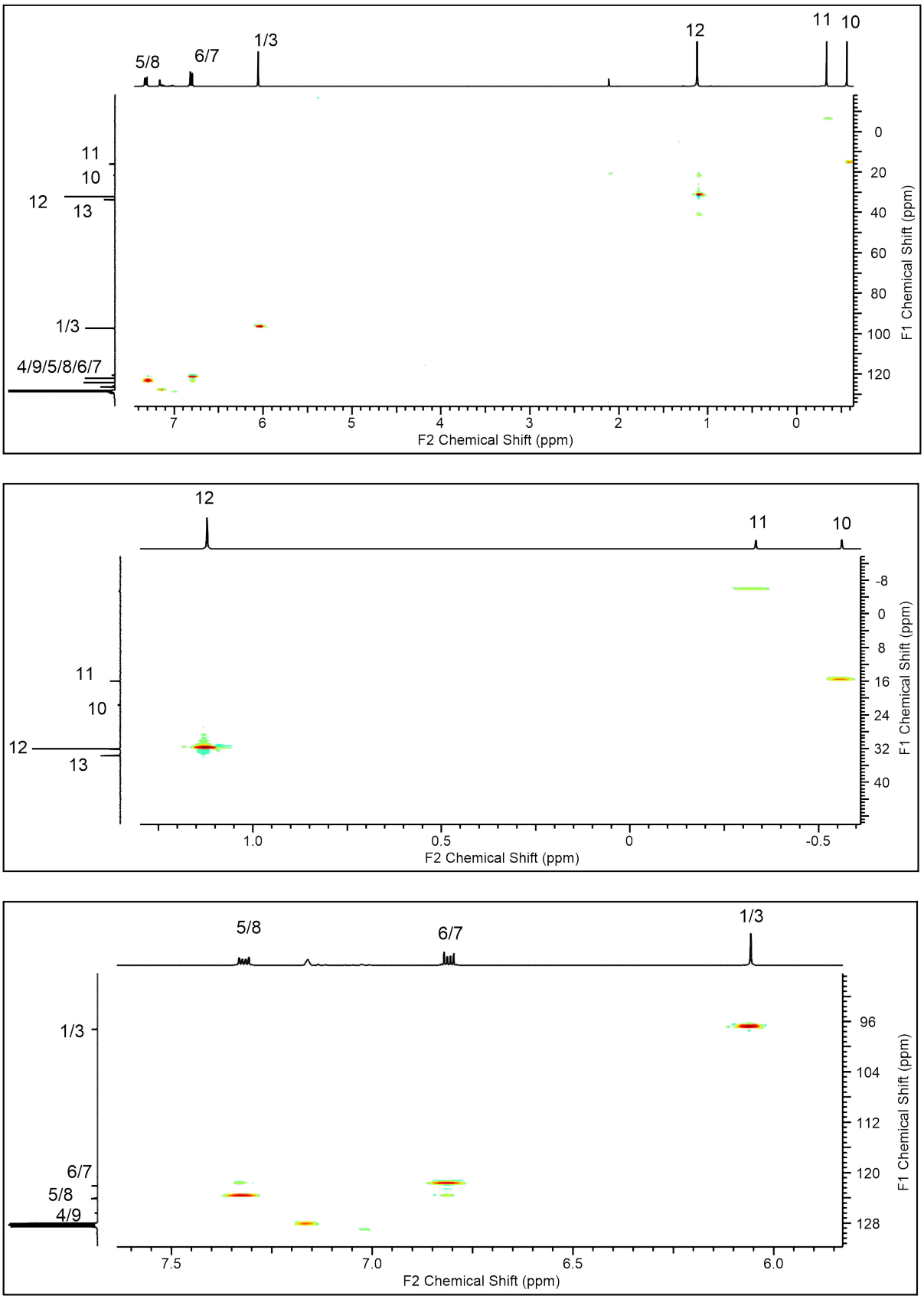

Figure S27. Section of $^{1}H^{13}C$-HSQC NMR spectrum (400/101 MHz) of $(Ind^{tBu})_2Lu(AlMe_4)$ (**2c**) in C_6D_6 at 26 °C, including enlarged sections.

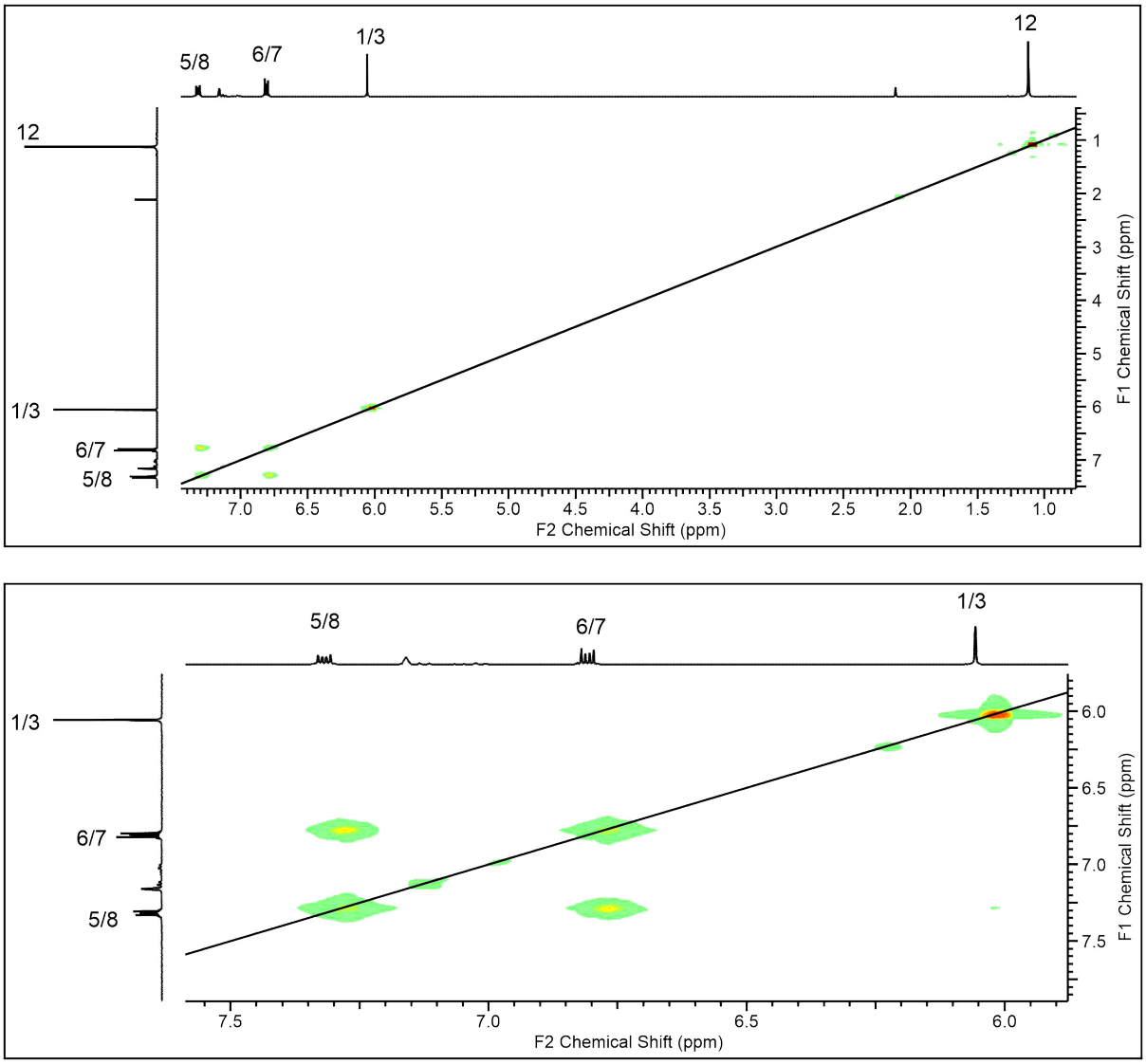

Figure S28. ^{1}H^{1}H-COSY NMR spectrum (400/400 MHz) of $(Ind^{tBu})_2Lu(AlMe_4)$ (**2c**) in C_6D_6 at 26 °C, including an enlarged section.

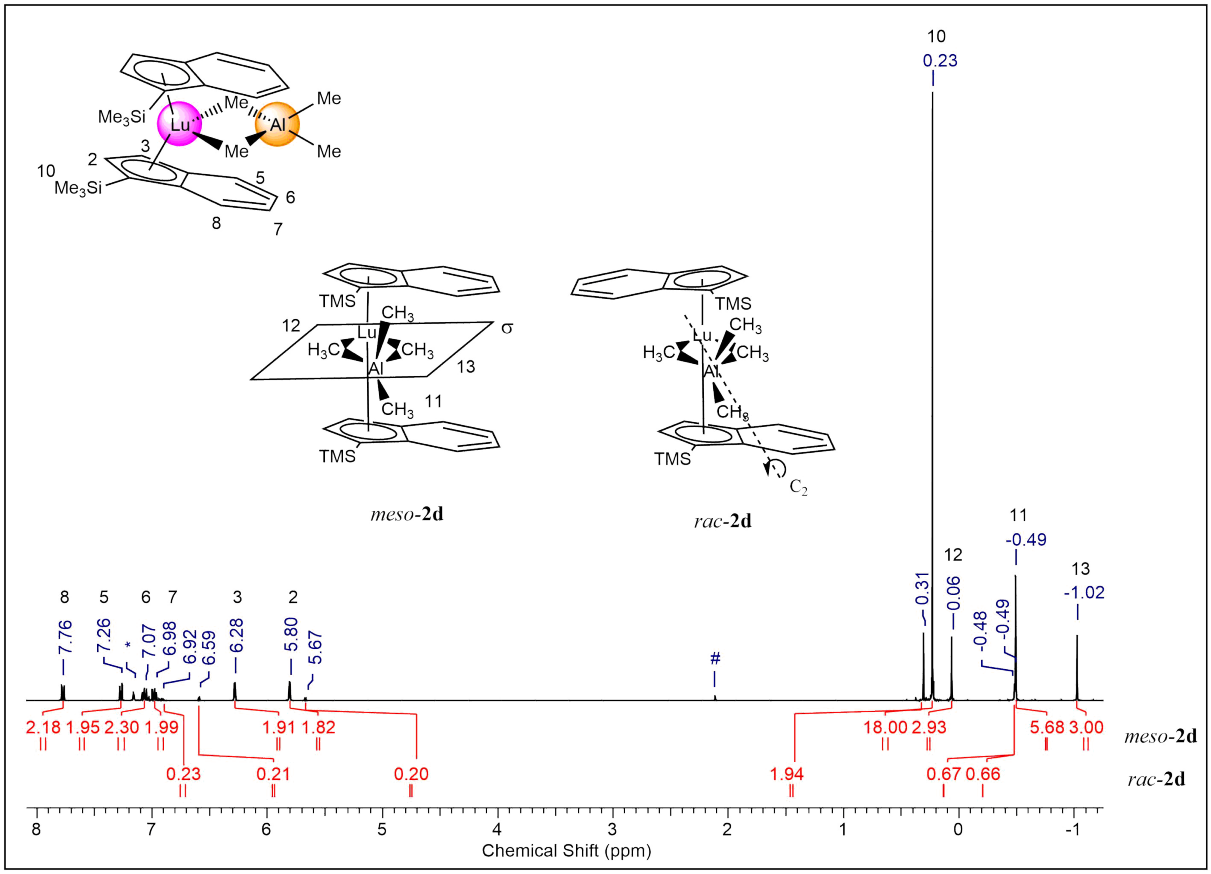

Figure S29. ^{1}H NMR spectrum (400 MHz) of $(Ind^{Si})_2Lu(AlMe_4)$ (**2d**) in C_6D_6 at 26 °C.

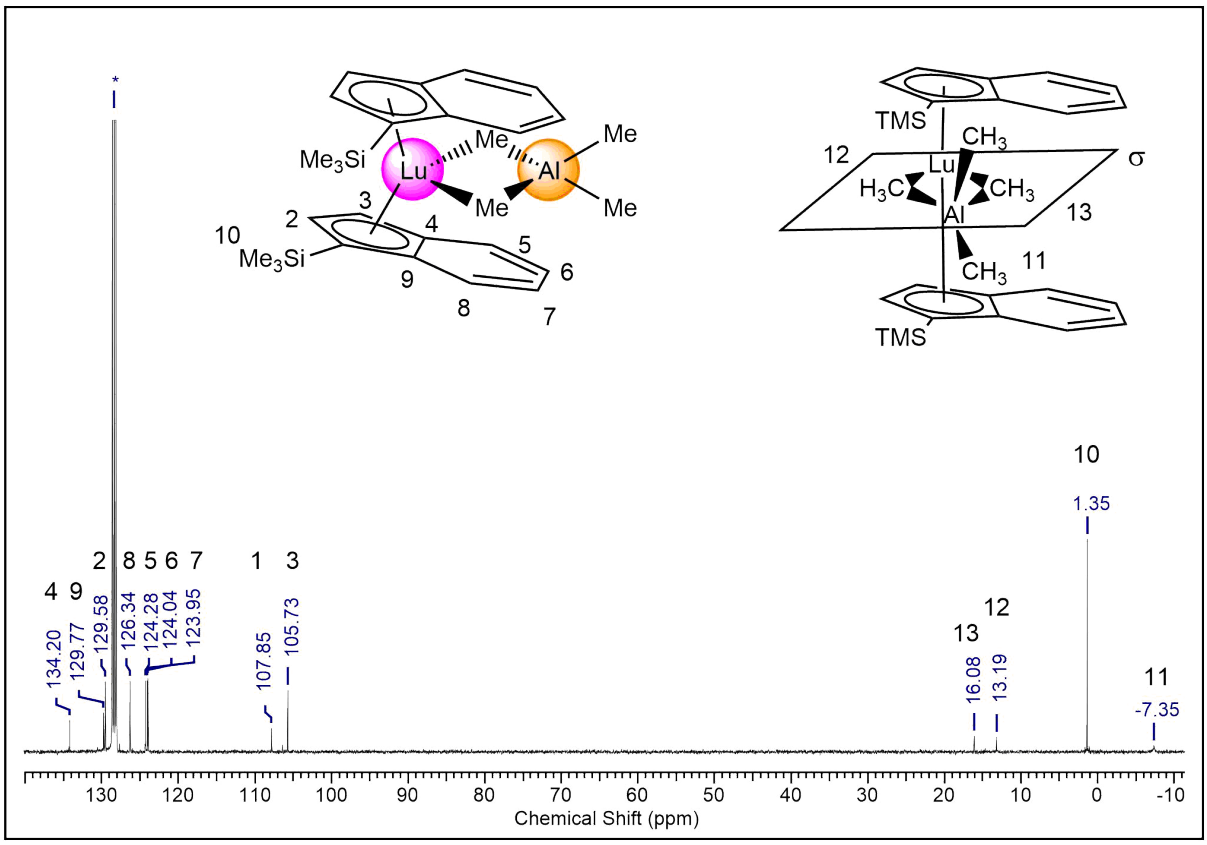

Figure S30. $^{13}C\{^{1}H\}$ NMR spectrum (101 MHz) of $(Ind^{Si})_2Lu(AlMe_4)$ (**2d**) in C_6D_6 at 26 °C.

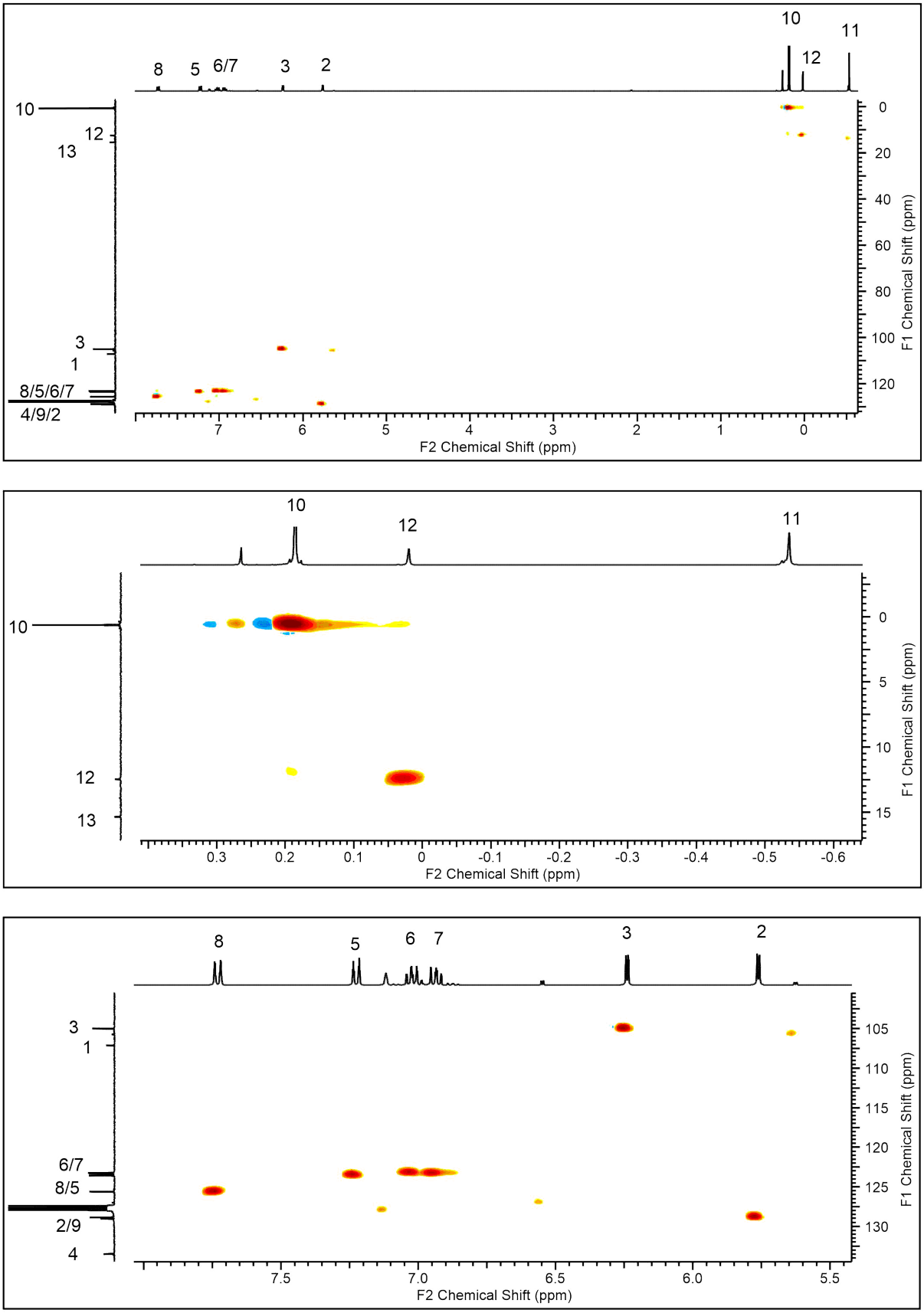

Figure S31. $^{1}H^{13}C$-HSQC NMR spectrum (400/101 MHz) of $(Ind^{Si})_2Lu(AlMe_4)$ (**2d**) in C_6D_6 at 26 °C, including enlarged sections.

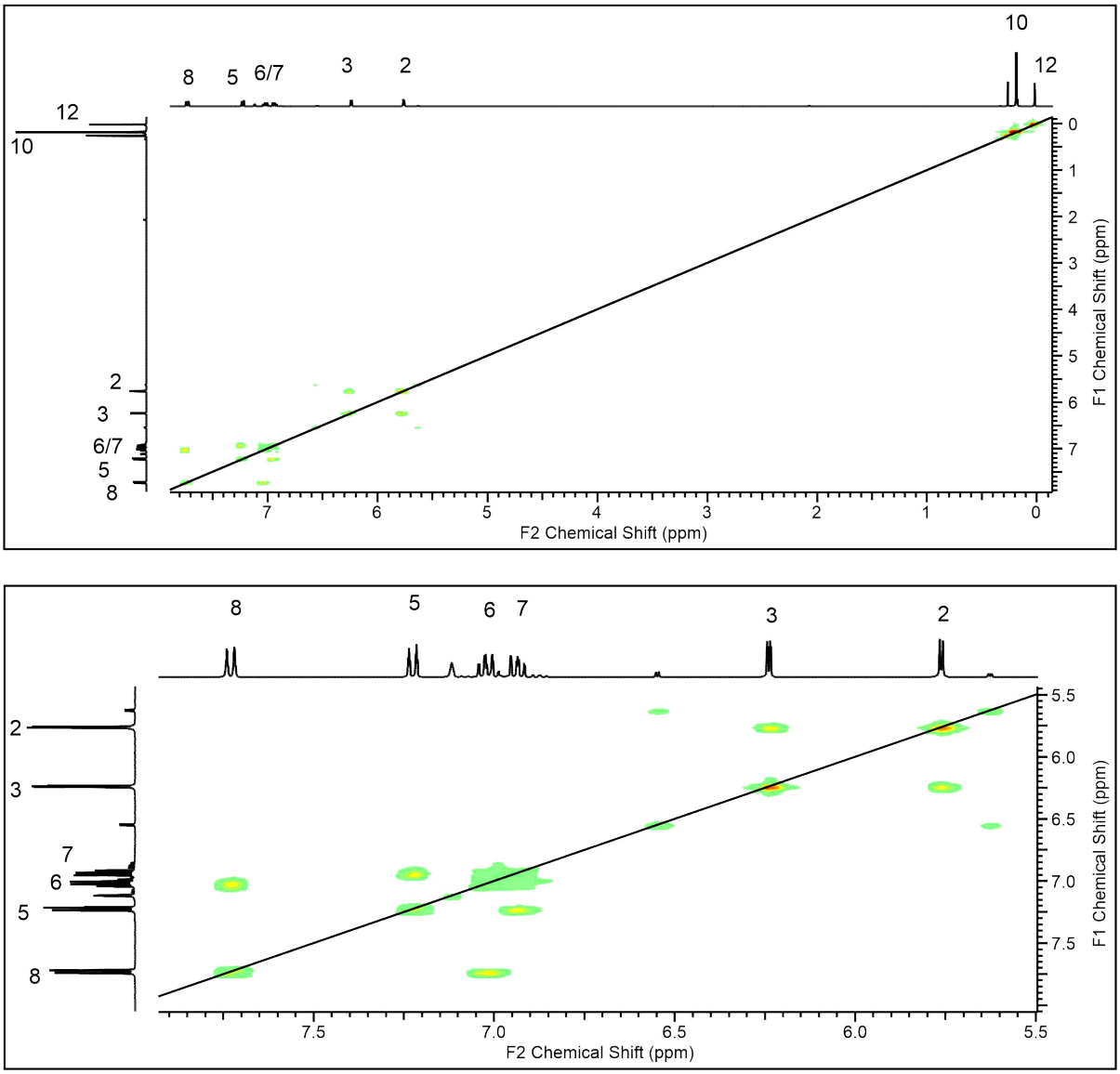

Figure S32. $^{1}H^{1}H$-COSY NMR spectrum (400/400 MHz) of $(Ind^{Si})_2Lu(AlMe_4)$ (**2d**) in C_6D_6 at 26 °C, including an enlarged section.

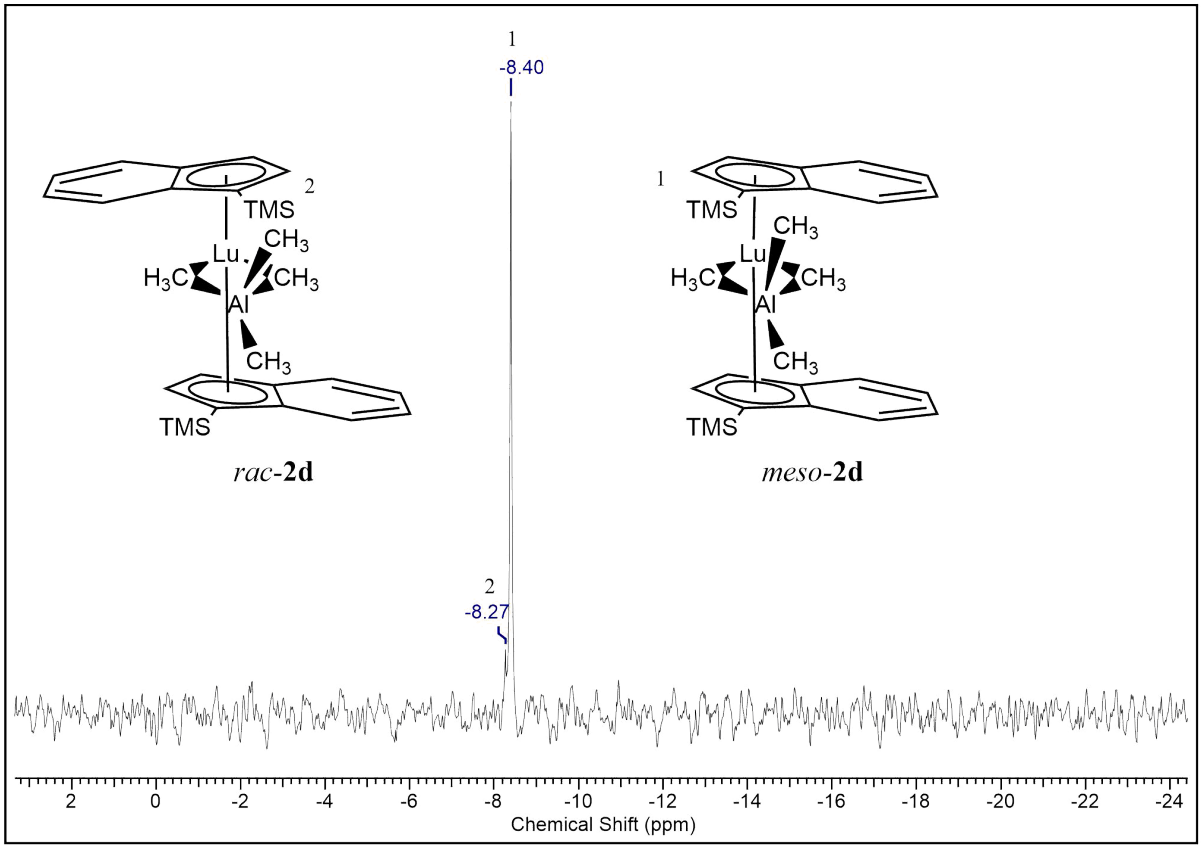

Figure S33. ^{29}Si-^{1}H DEPT45 NMR spectrum (50 MHz) of $(Ind^{Si})_2Lu(AlMe_4)$ (**2d**) in C_6D_6 at 26 °C.

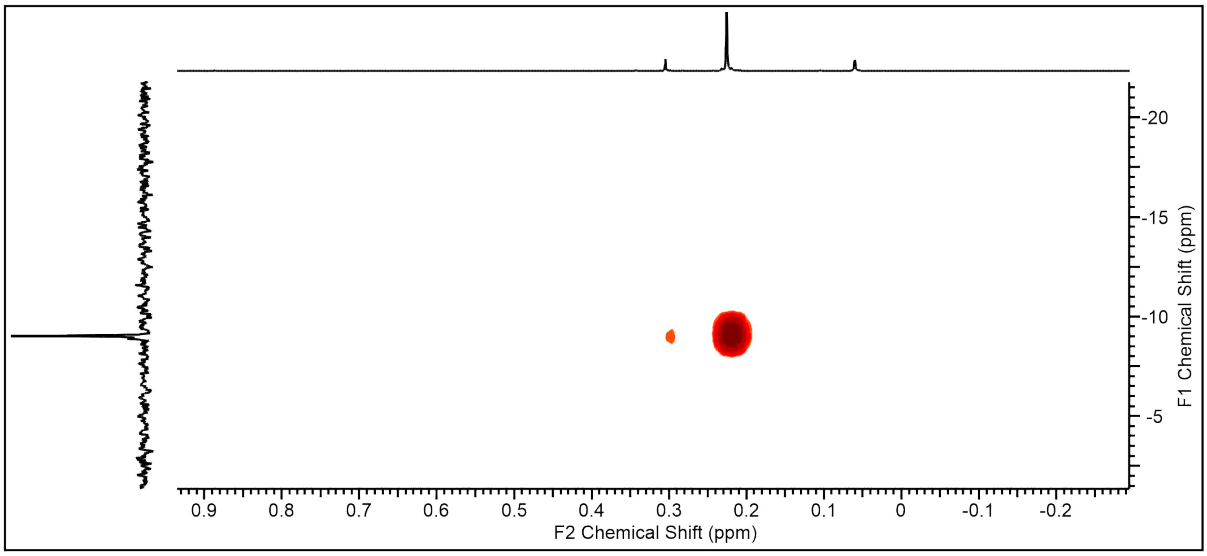

Figure S34. ^{1}H^{29}Si-HMBC NMR spectrum (500/99 MHz) of $(Ind^{Si})_2Lu(AlMe_4)$ (**2d**) in C_6D_6 at 26 °C.

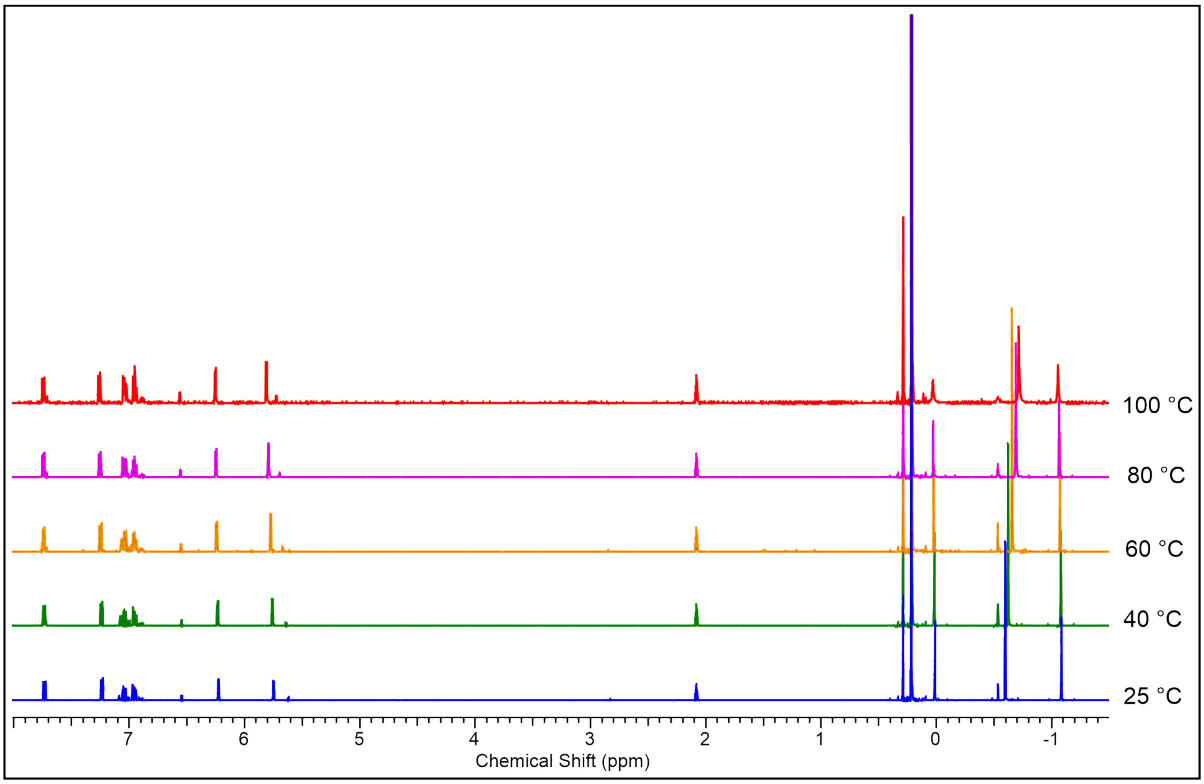

Figure S35. VT ^{1}H NMR spectrum (500 MHz) of $(Ind^{Si})_2Lu(AlMe_4)$ (**2d**) in tolune-*d8*. From 25 °C to 100 °C.

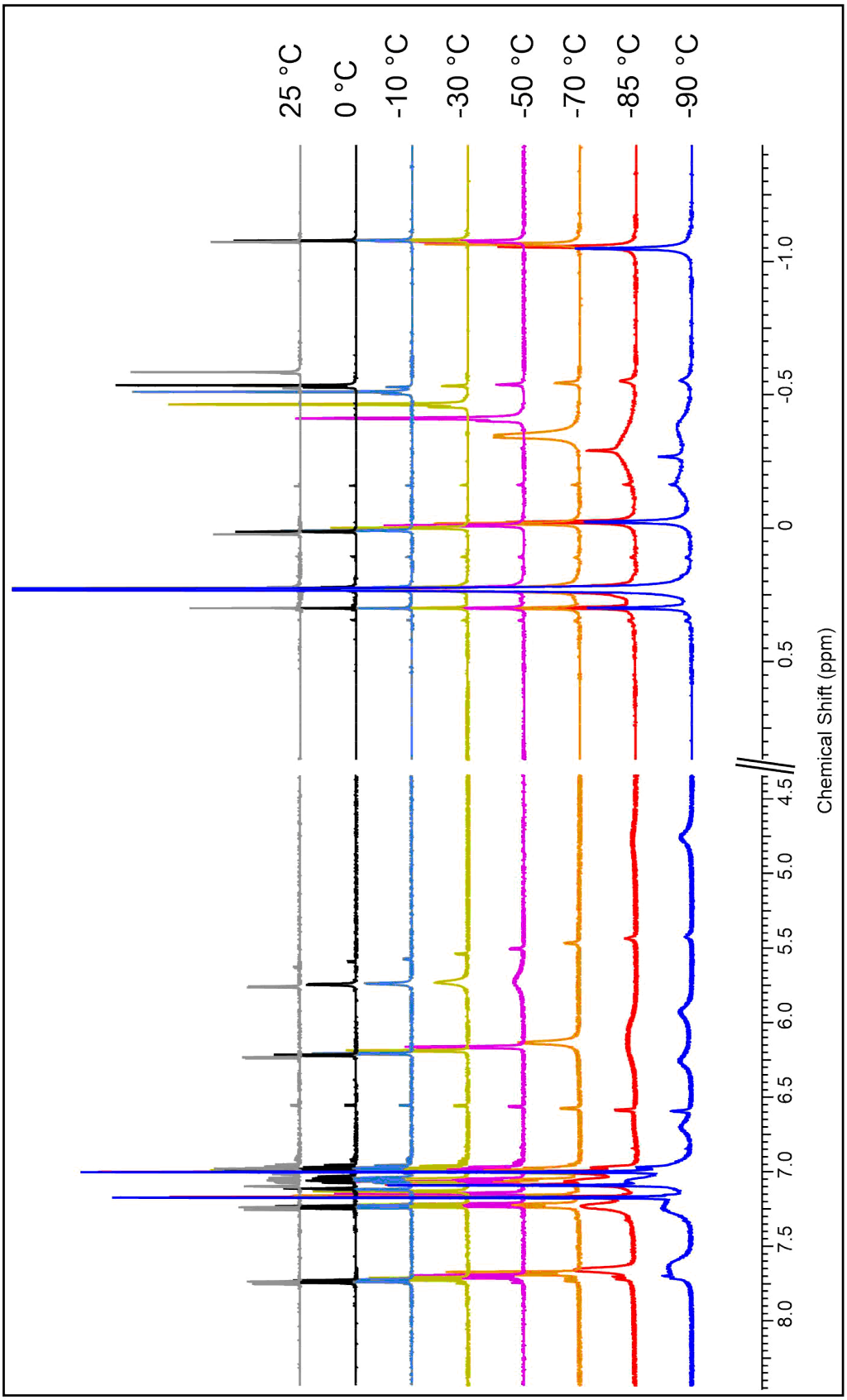

Figure S36. VT ^{1}H NMR spectrum (500 MHz) of $(Ind^{Si})_2Lu(AlMe_4)$ (**2d**) in tolune-*d8*. From –90 °C to 25 °C.

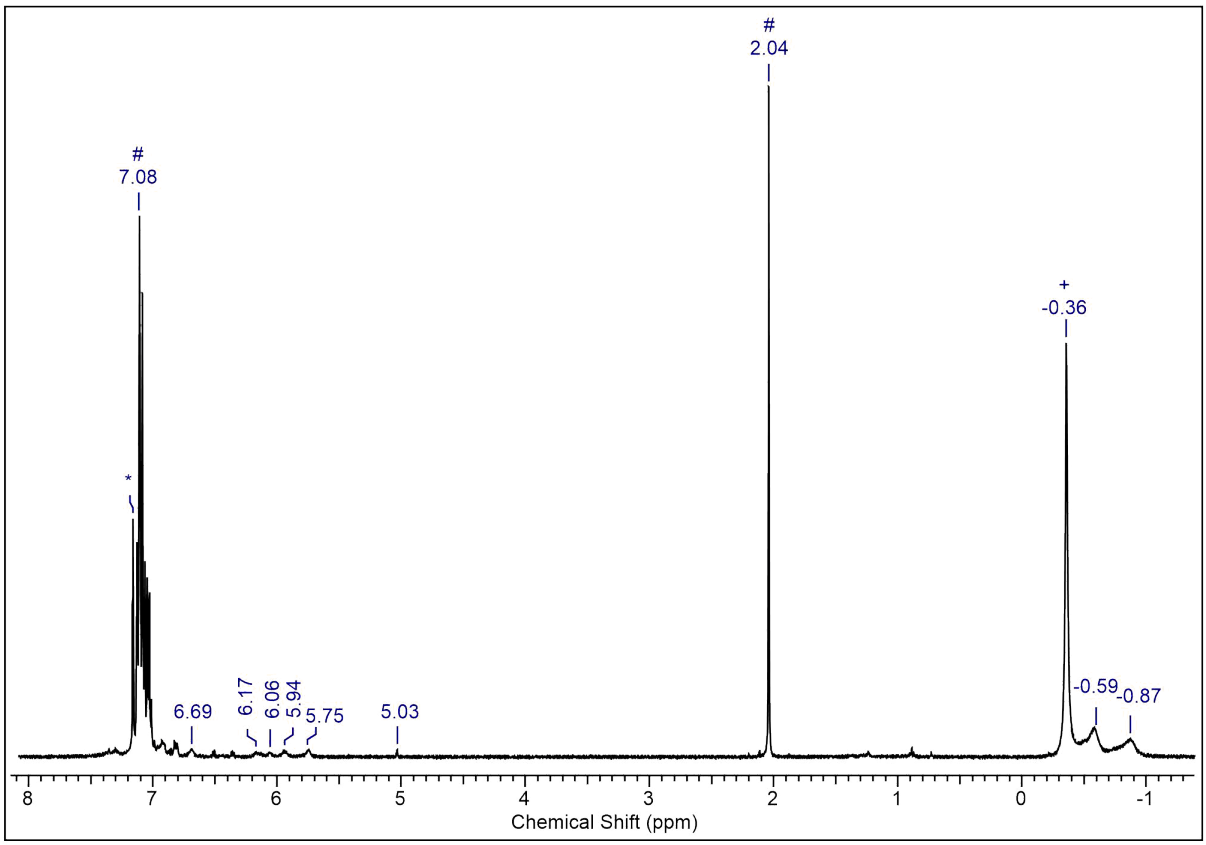

Figure S37. ^{1}H NMR spectrum (400 MHz) of the reaction of (Ind)La(AlMe$_4$)$_2$ (**1a**) with [Ph$_3$C][B(C$_6$F$_5$)$_4$] in C$_6$D$_6$ at 26 °C. Ph$_3$CMe is marked with #; free trimethylaluminum is marked +.

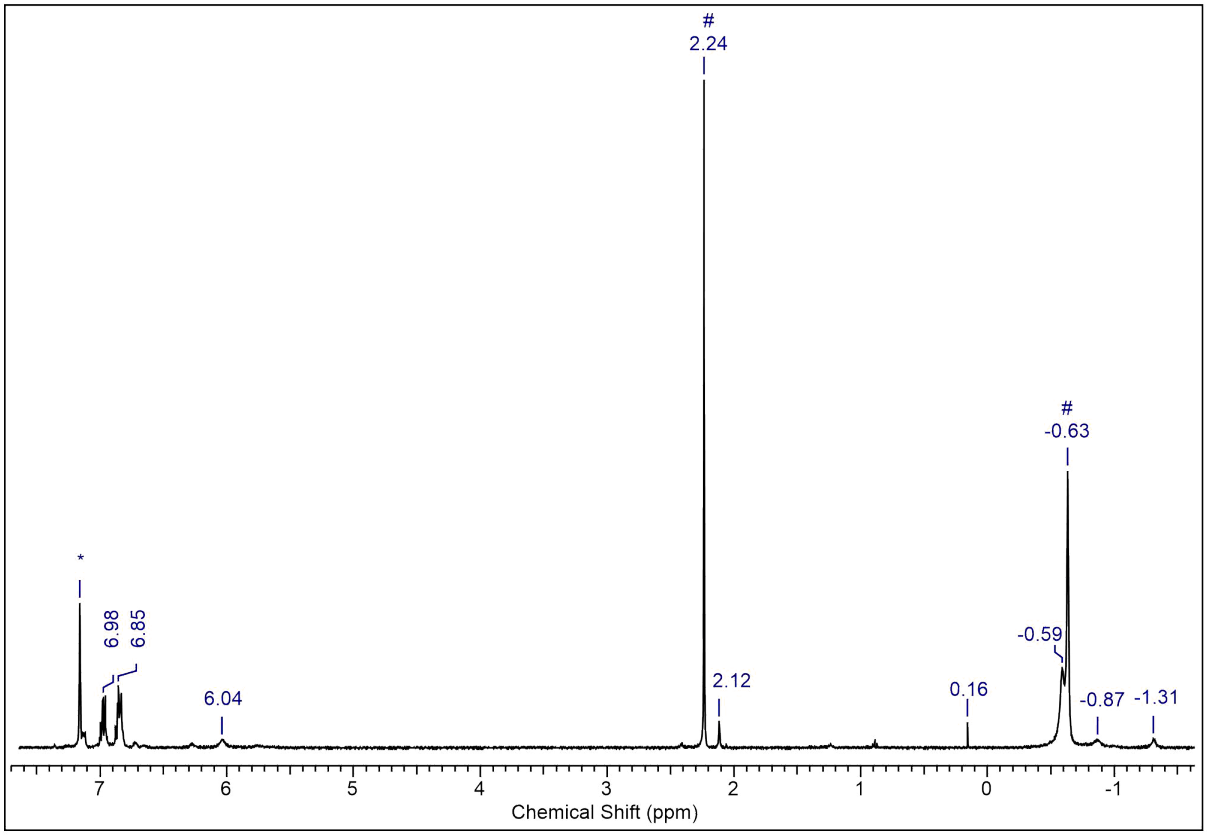

Figure S38. ^{1}H NMR spectrum (400 MHz) of the reaction of (Ind)La(AlMe$_4$)$_2$ (**1a**)with [PhNMe$_2$H][B(C$_6$F$_5$)$_4$] in C$_6$D$_6$ at 26 °C. PhNMe$_2$(AlMe$_3$) is marked with #.

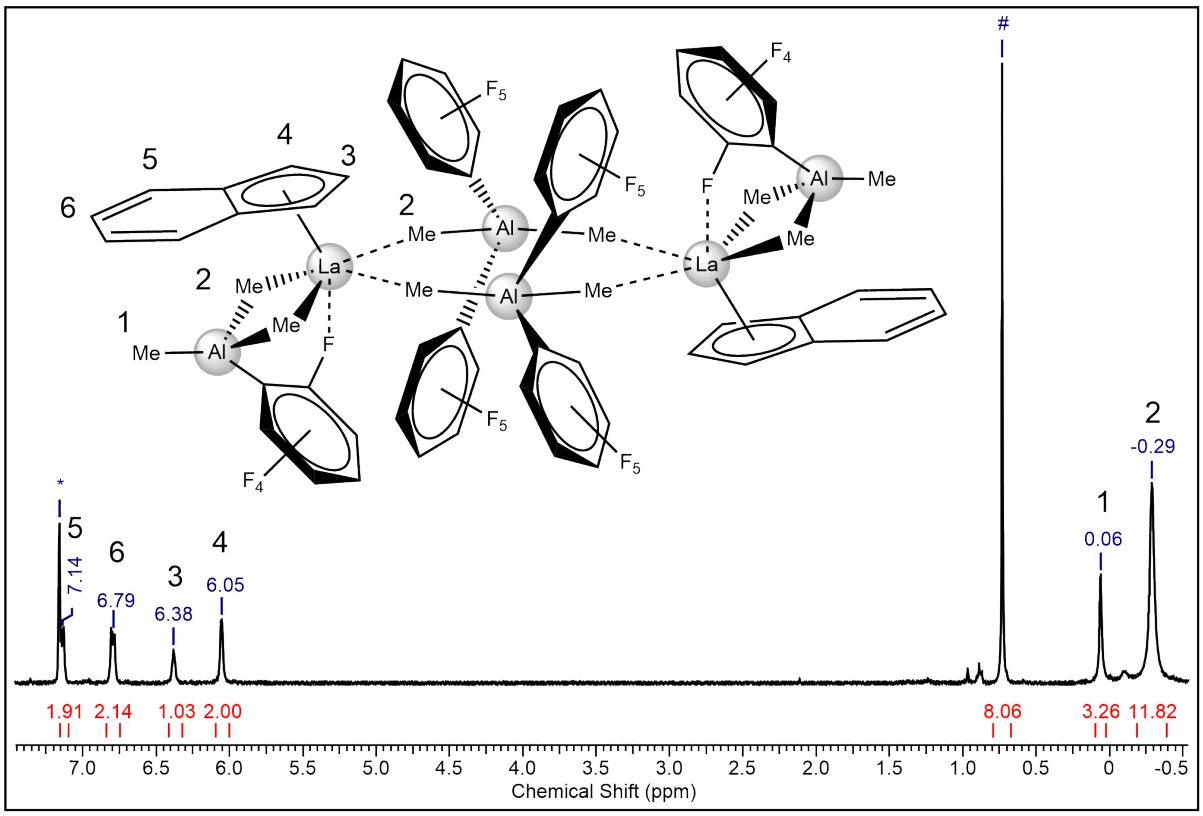

Figure S39. ^{1}H NMR spectrum (400 MHz) of the reaction of (Ind)La(AlMe$_4$)$_2$ with B(C$_6$F$_5$)$_3$ in C$_6$D$_6$ at 26 °C. BMe$_3$ is marked with #.

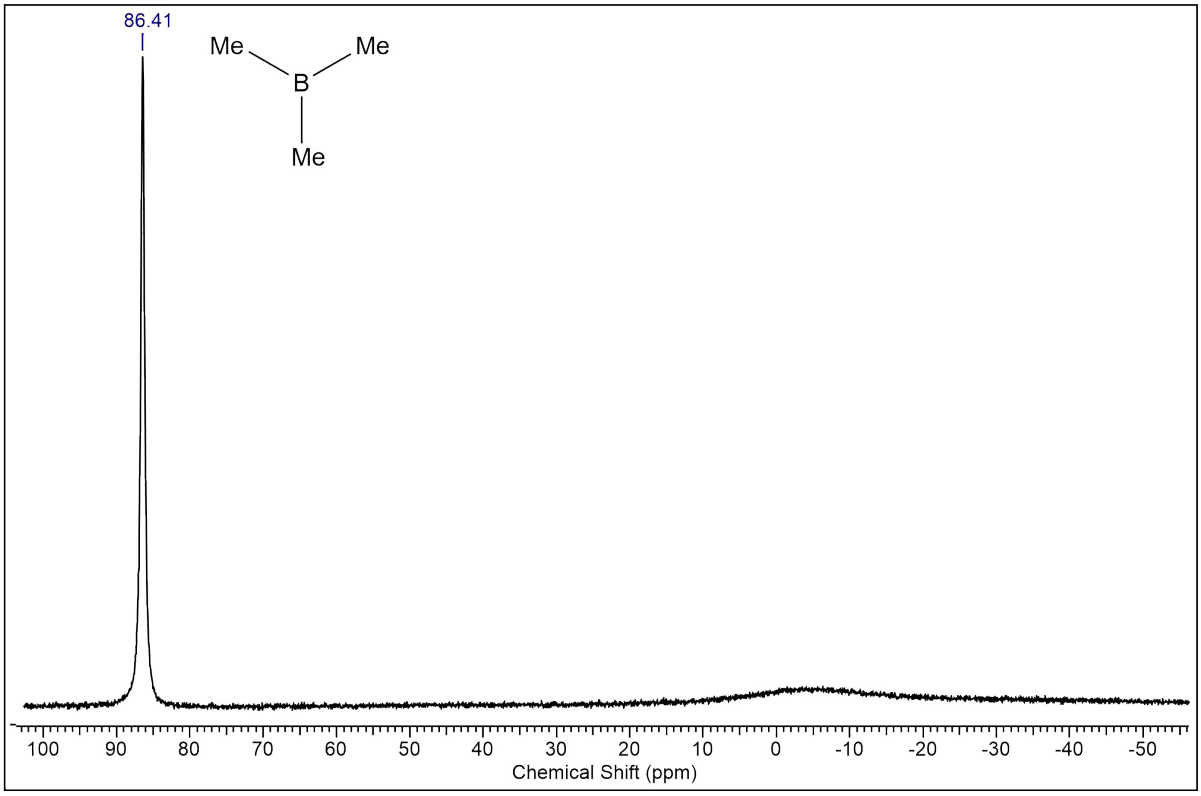

Figure S40. ^{11}B NMR spectrum (400 MHz) of the reaction of (Ind)La(AlMe$_4$)$_2$ with B(C$_6$F$_5$)$_3$ in C$_6$D$_6$ at 26 °C showing the formation of BMe$_3$.

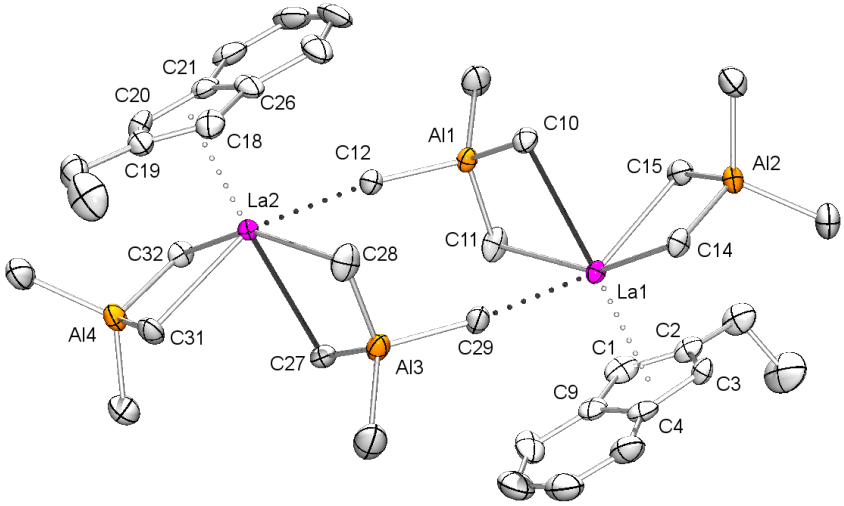

Figure S41. Molecular structure of $(Ind^{Et})La(AlMe_4)_2$ (**1b**). Hydrogen atoms are omitted for clarity. Atomic displacement parameters set at the 50% probability level. Selected bond lengths [Å] and angles [°]: La1–C1 2.781(5), La1–C2 2.836(4), La1–C3 2.792(4), La1–C4 2.815(5), La1–C9 2.803(5), La1–C10 2.967(5), La1–C11 2.757(5), La1–C14 2.694(5), La1–C15 2.714(5), La1···C29 2.966(5), La1···Al1 3.3821(15), La1···Al2 3.2214(16), C10-La1-C11 73.69(14), C14-La1-C15 79.22(15), La2–C18 2.796(5), La2–C19 2.885(5), La2–C20 2.798(4), La2–C21 2.794(5), La2–C26 2.797(5), La2–C27 2.912(5), La2–C28 2.787(5), La2–C31 2.695(5), La2–C32 2.714(5), La2···C12 2.974(4), La2···Al3 3.3606(16), La2···Al4 3.2380(17), C27–La2–C28 74.55(15), C31–La2–C32 78.77(15).

Table S1. Crystallographic Data for Compounds 1a, 1b, 1c, and 1d

	1a	**1b**	**1c**	**1d**
CCDC number	1915979	1915982	1915976	1915977
formula	$C_{20.5}H_{35}Al_2La$	$C_{19}H_{35}Al_2La$	$C_{21}H_{39}Al_2La$	$C_{20}H_{39}Al_2LaSi$
M [g·mol^{-1}]	474.35	456.34	484.39	500.47
Color	colorless	colorless	colorless	colorless
Crystal dimensions [mm]	0.234 x 0.170 x 0.096	0.175 x 0.161 x 0.085	0.528 x 0.457 x 0.244	0.480 x 0.244 x 0.188
Crystal system	monoclinic	orthorhombic	trigonal	triclinic
space group	$P2_1/c$	$Pca2_1$	$P3_1$	$P\bar{1}$
a [Å]	19.459(5)	19.545(3)	9.7198(5)	9.4353(5)
b [Å]	11.634(3)	10.1865(17)	9.7198(5)	9.6041(5)
c [Å]	21.681(6)	22.334(4)	22.1290(10)	15.4562(8)
α [°]	90	90	90	93.888(2)
β [°]	105.935(4)	90	90	103.960(2)
γ [°]	90	90	120	116.010(2)
V [Å^3]	4720(2)	4446.7(13)	1810.5(2)	1197.13
Z	8	8	3	2
T [K]	155(2)	150(2)	103(2)	100(2)
ρ_{calcd} [g·cm^{-3}]	1.335	1.363	1.333	1.388
μ [mm^{-1}]	1.884	1.997	1.843	1.908
F(000)	1928	1856	744	512
Unique reflns	13199	9267	7082	6161
Observed reflns	74853	90976	25431	35570
R1/*w*R2 (I>2σ)	0.0314/0.0604	0.0249/0.0450	0.0163/0.0407	0.0108/0.0288
R1/*w*R2 (all data)	0.0501/0.0683	0.0324/0.0472	0.0164/0.0407	0.0109/0.0289
Goodness of fit	1.022	1.038	1.077	1.080

Table S2. Crystallographic Data for Compounds 2a, 2b, 2c, and 2d

	2a	**2b**	**2c**	**2d**
CCDC number	1915980	1915981	1915978	1915983
formula	$C_{22}H_{26}AlLu$	$C_{26}H_{34}AlLu$	$C_{33.5}H_{46}AlLu$	$C_{28}H_{42}AlLuSi_2$
M [g·mol^{-1}]	492.38	548.48	650.65	636.74
Color	colorless	colorless	colorless	Colorless
Crystal dimensions [mm]	0.269 x 0.159 x 0.136	0.331 x 0.158 x 0.153	0.247 x 0.126 x 0.115	0.495 x 0.223 x 0.220
Crystal system	monoclinic	monoclinic	triclinic	monoclinic
space group	Cc	$P2_1/c$	$P\bar{1}$	$P2_1/c$
a [Å]	14.297(2)	13.9877(6)	9.915(4)	9.4943(13)
b [Å]	14.304(2)	18.5367(8)	10.487(6)	16.796(2)
c [Å]	19.222(3)	9.3019(4)	15.091(5)	18.475(3)
α [°]	90	90	75.814(11)	90
β [°]	97.286(2)	103.447(2)	81.200(6)	98.438(4)
γ [°]	90	90	77.448(11)	90
V [Å^3]	3899.1(11)	2345.73(18)	1476.6(11)	2914.2(7)
Z	8	4	2	4
T [K]	150(2)	100(2)	100(2)	100(2)
ρ_{calcd} [g·cm^{-3}]	1.678	1.553	1.463	1.451
μ [mm^{-1}]	5.108	4.254	3.392	3.513
F(000)	1936	1096	662	1288
Unique reflns	9619	6586	8656	7837
Observed reflns	29878	58663	63482	44485
R1/*w*R2 (I>2σ)	0.0221/0.0514	0.0144/0.0342	0.0204/0.0482	0.0172/0.0415
R1/*w*R2 (all data)	0.0227/0.0516	0.0163/0.0350	0.0228/0.0491	0.0185/0.0420
Goodness of fit	1.092	0.982	1.106	1.075

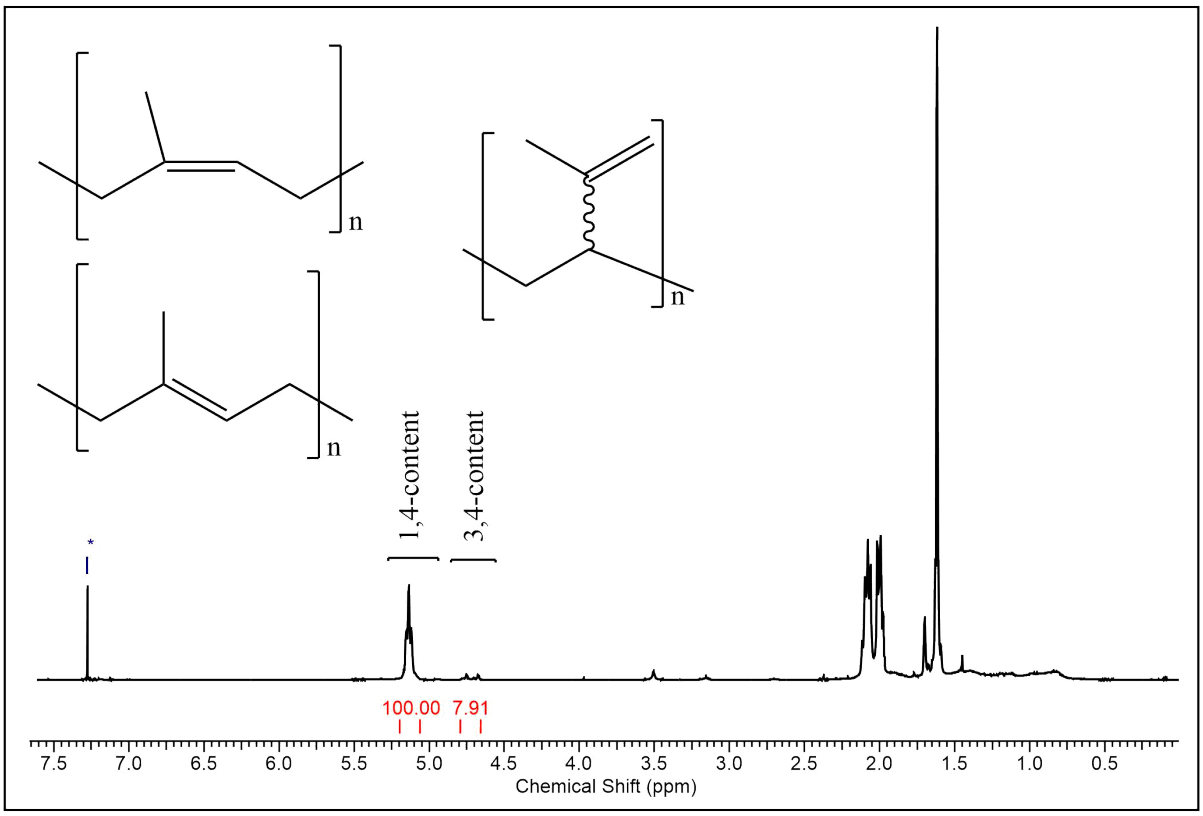

Figure S42. ^{1}H NMR spectrum (400 MHz) of polyisoprene (entry 4) in $CDCl_3$ at 26 °C.

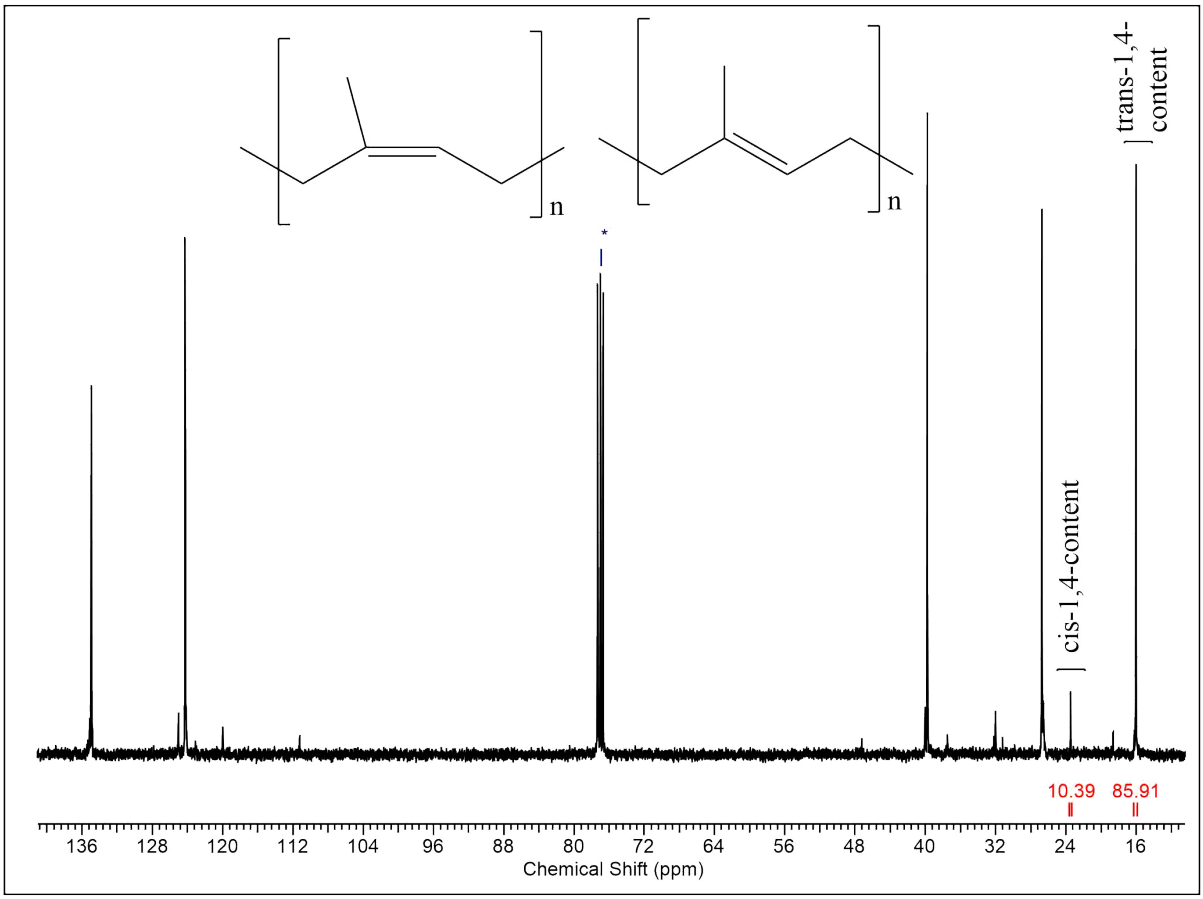

Figure S43. ^{13}C{^{1}H} NMR spectrum (101 MHz) of polyisoprene (entry 4) in $CDCl_3$ at 26 °C.

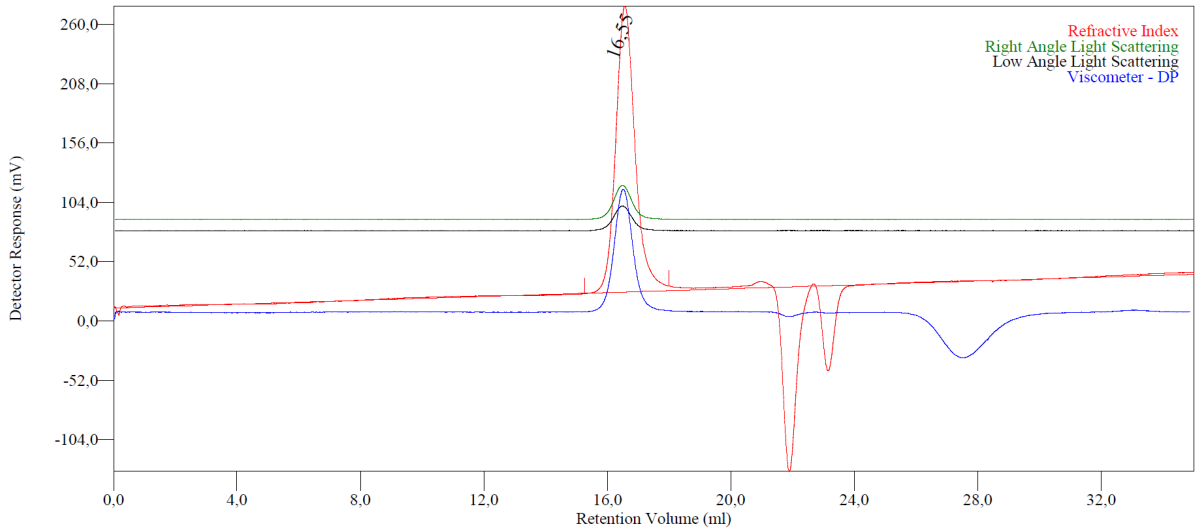

Figure S44. GPC curve of polyisoprene (entry 4).

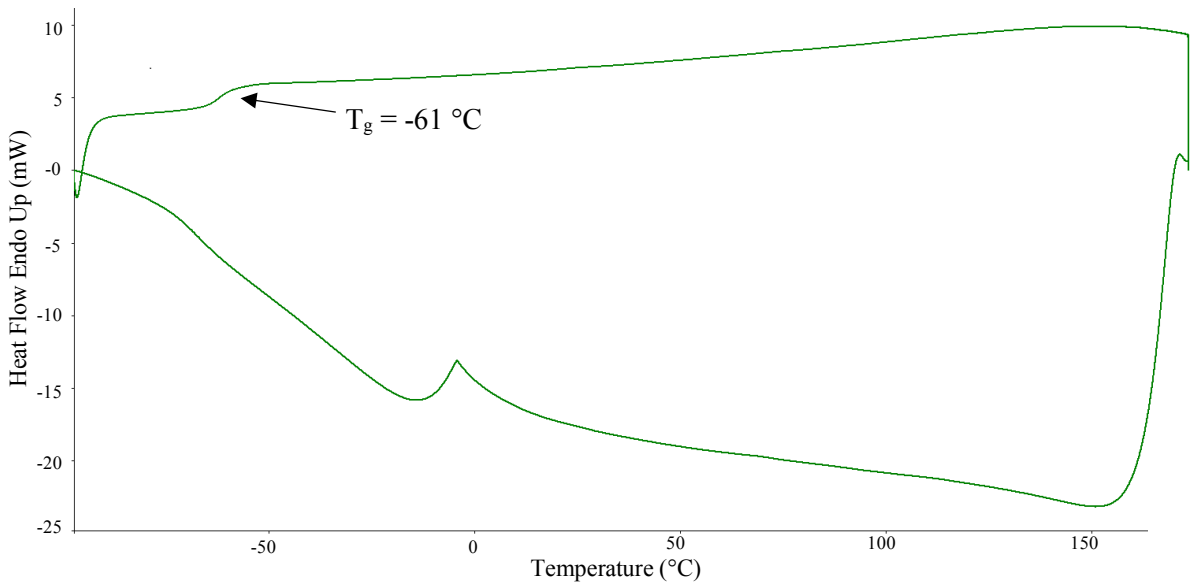

Figure S45. DSC curve of polyisoprene (entry 4).

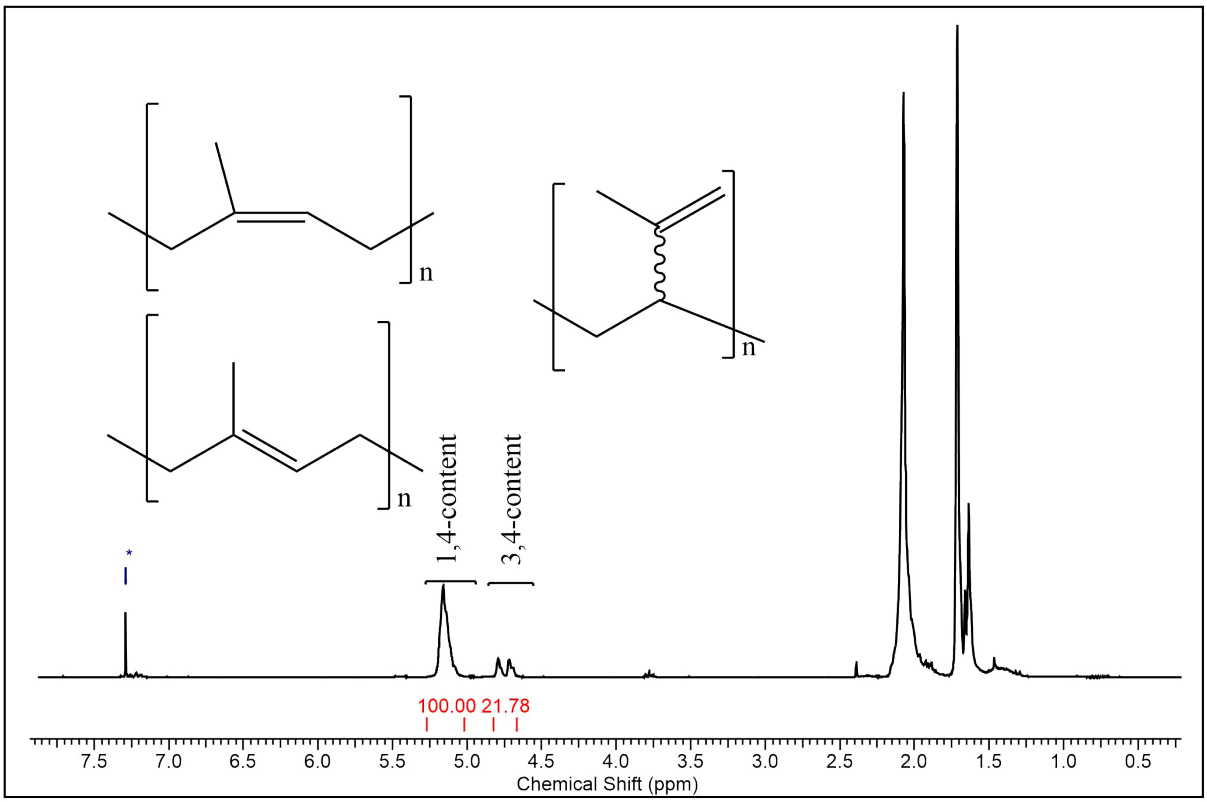

Figure S46. ^{1}H NMR spectrum (400 MHz) of polyisoprene (entry 14) in $CDCl_3$ at 26 °C.

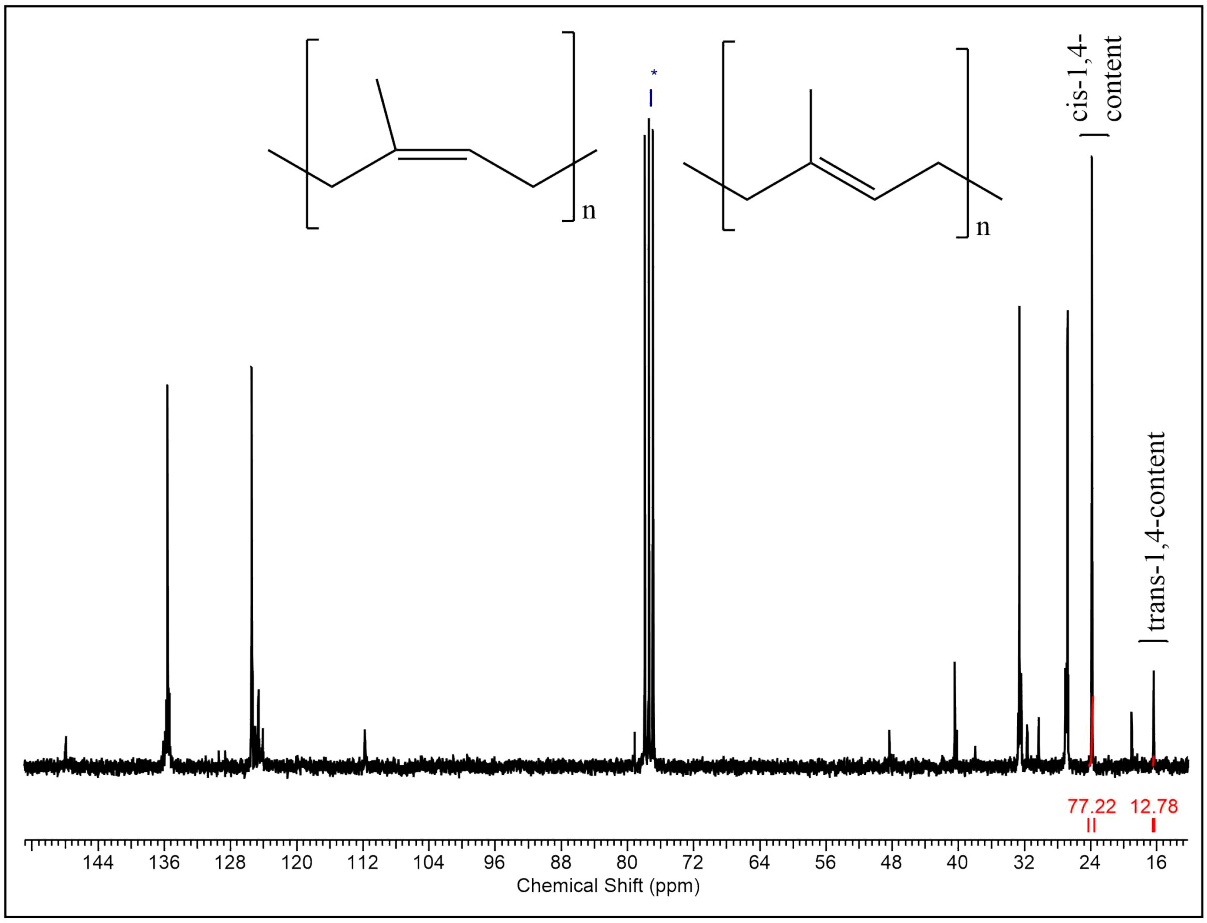

Figure S47. ^{13}C{^{1}H} NMR spectrum (101 MHz) of polyisoprene (entry 14) in $CDCl_3$ at 26 °C.

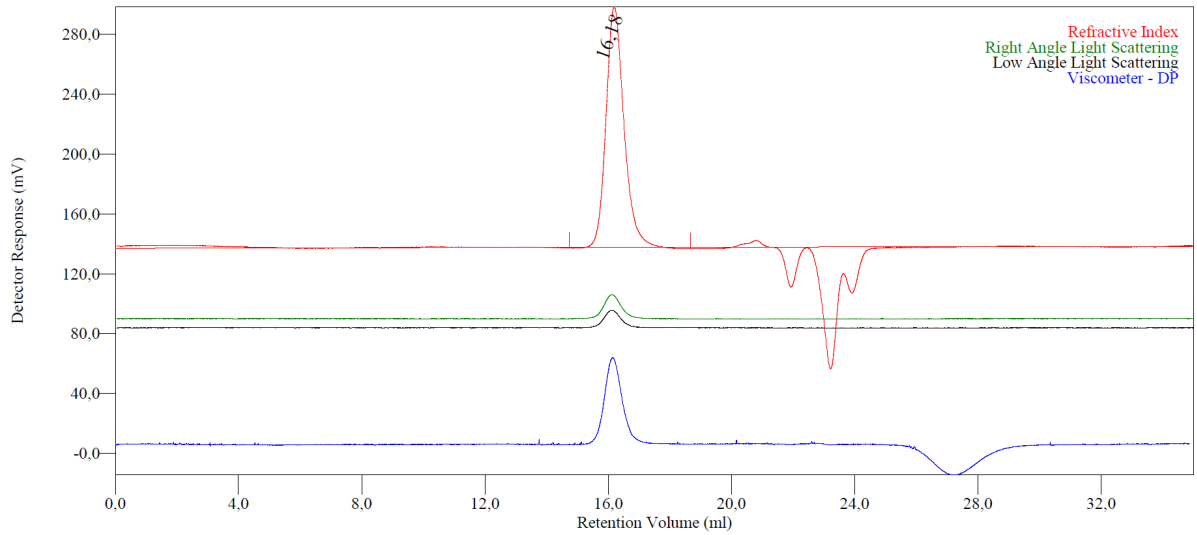

Figure S48. GPC curve of polyisoprene (entry 14).

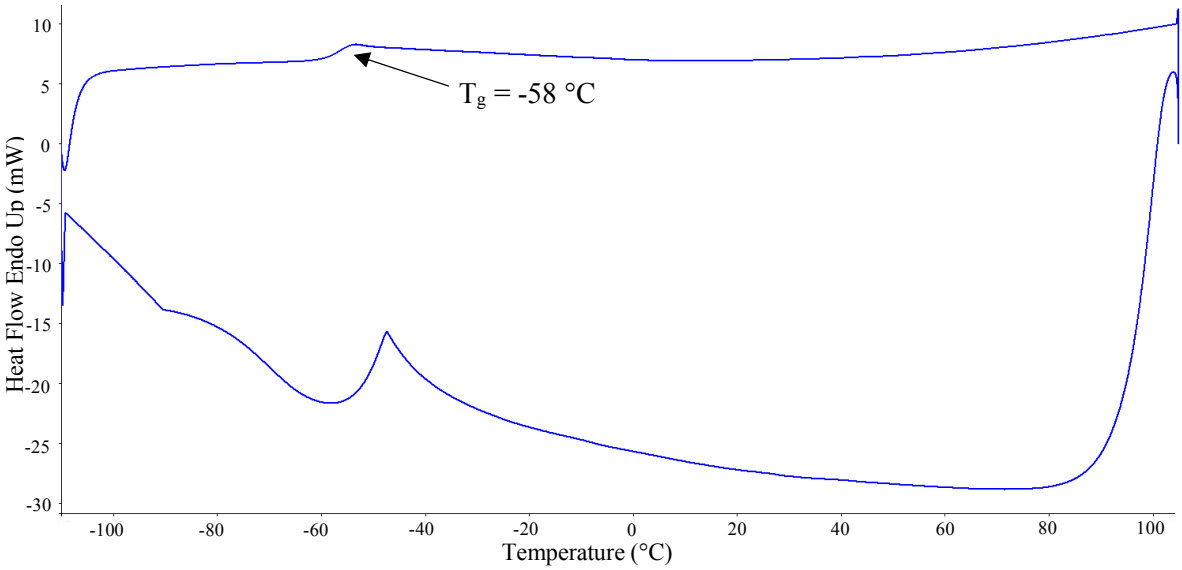

Figure S49. DSC curve of polyisoprene (entry 14).